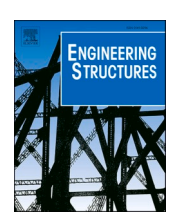
ELSEVIER

Contents lists available at ScienceDirect

Engineering Structures

journal homepage: www.elsevier.com/locate/engstruct





Three-dimensional nonlinear displacement-based beam element for members with angle and tee sections

Xinlong Du^a, Jerome Hajjar^b

- ^a Department of Civil and Environmental Engineering, Northeastern University, Boston, MA 02115, USA
- ^b CDM Smith Professor and Chair, Department of Civil and Environmental Engineering, Northeastern University, Boston, MA 02115, USA

ARTICLE INFO

Keywords:
Asymmetric section
Corotational transformation
Displacement-based element
Green-Lagrange strain
Axial-flexural-torsional interaction
Membrane locking
Fiber section

ABSTRACT

Asymmetric thin-walled sections such as steel angles and tees are widely used in a range of steel structures. To address extreme limit states that these structures encounter due to extreme events such as hurricanes and earthquakes, it is important to capture their response due to large deformations caused by static or dynamic loading. In the nonlinear large deformation regime, these members have coupled axial-flexural-torsional deformation due to the so-called Wagner effect and the noncoincident shear center and centroid. A threedimensional corotational total Lagrangian beam element is formulated and implemented in the OpenSees corotational framework to account for these coupling effects by invoking Green-Lagrange strains referenced to a basic system. In the basic system, shear forces and torque are defined with respect to the shear center, axial force is referred to the centroid, and flexure is defined around the section principle axes but in the planes containing the shear center. The element tangent stiffness matrix is derived through linearization of the governing equation obtained from the principle of virtual work. Cubic Hermitian functions for the transverse displacements and a linear shape function for the axial and torsional deformation are adopted in the development. Before conducting the corotational transformation, all element end forces and displacements are transformed to act about the shear center. In order to remedy membrane locking in the inextensional bending mode, the high order bending terms in the axial strain are replaced by a constant effective strain. Cyclic material nonlinearity is considered by discretizing the cross section into a grid of fibers, tracking the steel uniaxial stress-strain constitutive at each fiber, and performing numerical integration over the cross section to obtain the section stiffness matrix. The formulation is compared against a set of experimental and numerical results to validate that the element can model geometric and material nonlinearities accurately and efficiently.

1. Introduction

The conventional approaches developed to address the mechanics of structural beam elements are often based on the assumption that different deformation modes (axial, bending and torsion) are independent. However, for a three-dimensional structural member, this assumption is only acceptable for small deformations and only if the member has a doubly symmetric cross section. For nonlinear large deformations, this assumption breaks down even for members with doubly symmetric sections, because different modes of deformation may be coupled. To consider these coupling effects accurately, several phenomena need to be taken into account, such as the so-called Wagner effect, and the coupling caused by the noncoincident shear center and centroid of asymmetric cross sections. In finite element analysis, these coupling effects usually are modeled through including of the geometric

stiffness matrix, which is usually obtained using three approaches: a total Lagrangian formulation, an updated Lagrangian formulation and a corotational formulation [1–5]. In the total Lagrangian formulation, the initial undeformed configuration is selected as the reference state, whereas in the updated Lagrangian formulation, the last calculated configuration is adopted for the same purpose [6]. In the corotational formulation, a basic coordinate system is lined up with each element chord and continuously translates and rotates with the element as the deformations proceed [7]. The element is formulated in the basic system then transformed to the global system through the corotational transformation.

For members with thin-walled sections, the geometric nonlinear behavior is more complex than the coupling of axial, bending and torsional deformations. This is because other effects, such as local buckling, section distortional buckling, and variable warping are

E-mail addresses: du.xinl@northeastern.edu (X. Du), jf.hajjar@northeastern.edu (J. Hajjar).

present. Buckling analysis of members with thin-walled sections has been studied extensively in the literature with consideration of the warping effect [8–13]. The local and distortional buckling effects can be included in beam elements by employing generalized beam theory (GBT) models [14–18] or using deformation-specific tangent rigidities to account for loss of stiffness as proposed by Rasmussen et al. [19–21]. Since the present element is developed for analyzing steel structures made of hot-rolled steel angles and tees, this paper only focuses on coupled axial, flexural and torsional buckling.

Kitipornchai and Chan [22] and Chan and Kitipornchai [23] derived element geometric stiffness matrices for angle and tee beam-columns, as well as for generic asymmetric thin-walled beam-columns. An updated Lagrangian formulation, coupled with the arc-length technique for iterative solution at each step, was adopted to trace the nonlinear load-deformation relationship. The effectiveness and accuracy of this formulation was demonstrated using different examples, for which the buckling loads and the load-deformation relationships were developed. The material was assumed to be linear elastic. In later work, they introduced a lumped plasticity approach, coupled with the concept of a yield surface in stress-resultant space, to model the material nonlinearity of thin-walled structures [24].

Lee and McClure [25] developed a three-dimensional L-section beam finite element for elastoplastic large deformation analysis. They proposed a generalized interpolation scheme for the isoparametric formulation of a three-dimensional thin-walled beam element. The updated Lagrangian formulation was adopted considering large deformation behavior. The axial, bending and shearing actions were included and the 'mixed interpolation of tensorial components' (MITC) technique was used for the locking removal. In order to address eccentricities in the element for loading and displacement, the longitudinal reference line can be positioned arbitrarily on the beam section. However, the eccentricities were implemented in the element derivation, which means the users cannot specify the eccentricities by themselves.

Recently, Liu et al. [26] developed an efficient beam element implementation within the educational structural analysis software MASTAN2 [27], which is capable of doing large-deformation analysis of thin-walled members with asymmetric sections and modeling the Wagner effects. The updated Lagrangian method was adopted for the large deflection analysis. Then, they improved derivations and validations for the element linear and geometric stiffness matrices [28]. This work also showed the calculation details of a refined cross-section analysis algorithm for arbitrarily-shaped open sections. Linear elastic material is assumed throughout their work.

There are other researchers who developed beam-column elements with asymmetric sections under the corotational framework. Hsiao and Lin [29] and Chen et al. [30] derived a corotational total Lagrangian element formulation for geometric nonlinear analysis of thin-walled members with monosymmetric and asymmetric cross sections and linear elastic materials. Battini and Pacoste [31,32] proposed the formulation of three-dimensional corotational beam elements for buckling and post-buckling analysis of frame structures, where the centroid and shear center of the cross section are not necessarily coincident. More recently, Rinchen et al. [33,34] derived a displacementbased beam element formulation for asymmetric thin-walled members, which was implemented in the OpenSees corotational framework [35]. In the work of Rinchen et al. [33,34], membrane locking occurs because linear and cubic shape functions are used for axial and lateral displacements, respectively, which may cause the element to overestimate the bending stiffness when the beam section is thin or the element geometry becomes curved [4,36]. In addition to the conventional corotational approach, which is applied to a whole finite element, Garcea et al. [37,38] proposed the Implicit Corotational Method (ICM), in which a corotational frame is introduced for each point on the beam axis. Genoese et al. [39] then utilized the ICM in a geometrically nonlinear beam element for members with generic sections.

In this paper, a displacement-based beam element is developed

following the corotational total Lagrangian formulation. Rigid body motions are considered in the corotational transformation, while element deformations with geometric nonlinear effects are modeled in the basic system through the total Lagrangian approach. The basic system and beam section kinematics used in the original OpenSees corotational framework is modified to consider the noncoincident centroid and shear center. The fiber section method with uniaxial constitutive laws for each fiber is utilized to model the distributed inelastic behavior. Compared to the work of Battini and Pacoste [31,32], this research adopts a different kinematic model, which decouples axial, flexural and torsional deformations in the basic system [22,23] and follows the classical beam theory where bending is referred to the centroid and torsion is defined with respect to the shear center. On the contrary, deformations are coupled for the kinematic model used by Battini and Pacoste [31,32], which is not considered in the interpolations of deformations. Thus, a more accurate displacement field can be obtained if the proposed kinematic model with the same interpolation functions is used. As shown in Section 4, fewer of the elements developed in this work are needed to obtain comparable accuracy with the element developed by Battini and Pacoste [31,32]. Due to this kinematic model, a cross-section transformation matrix is utilized in advance of the corotational transformation to move all degrees-of-freedom (DOFs) to act about the member reference axis. Compared to the work of Rinchen et al. [34], in this research membrane locking is remedied through a special treatment of the higher order terms in the Green-Lagrange strain; in addition, the cross-section transformation matrix and the shape functions are improved. Finally, a number of members and systems are analyzed to validate the accuracy of the results from the implementation within the OpenSees software.

2. Geometric nonlinear analysis formulation

The corotational transformation decomposes the motion of the element into rigid body movements and pure deformations, through the use of a basic coordinate system attached to the current deformed configuration as the reference system, which continuously rotates and translates with the element. Within the basic system, a geometric linear formulation, a total Lagrangian formulation or an updated Lagrangian formulation can be adopted [29,30,40]. OpenSees employs the corotational transformation with a geometric linear formulation in the basic system for developing nonlinear displacement-based beam elements. Consequently, the high order terms in the strain displacement relationship are neglected in the basic system, which means that the axial, flexural and torsional deformations are independent of each other in the basic system. The axial-flexural interaction can be captured in the global system by the corotational transformation; however, the axial-torsional and flexural-torsional interaction cannot be recovered in the global system. Therefore, the torsional behavior is independent to axial and flexural deformations for the original displacement-based beam element in OpenSees, which leads to the inability of this element to simulate torsional and flexural-torsional buckling behavior of members. In this research, the high order terms in the strain displacement compatibility equation are included through the total Lagrangian formulation in the basic system of the corotational transformation formulation. A brief introduction of this total Lagrangian corotational formulation is presented in this section.

2.1. Total Lagrangian formulation

Fig. 1 shows the concept of the total Lagrangian method applied to a 3D beam element. In the total Lagrangian formulation, when describing strains and displacements, the reference configuration is the initial configuration at time 0. The element is formulated in the 12-DOF local system of the initial configuration, then transformed to the global system using the transformation matrix of the initial configuration. The transformation matrix is constant for each element. There are 12 DOFs in the

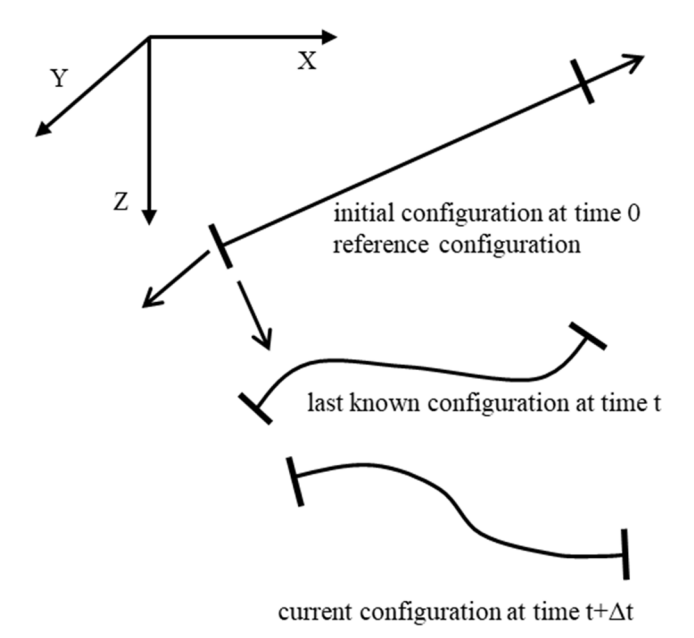


Fig. 1. Illustration of the total Lagrangian formulation (after Mattiasson et al. [7]).

local system because element ends have lateral displacements and rotations.

Theoretically, the principle of virtual work at time $t + \Delta t$ is

$$\int_{t+\Delta t} \int_{t+\Delta t} \tau_{ij} \delta_{t+\Delta t} e_{ij}^{t+\Delta t} dV = {}^{t+\Delta t} \mathscr{R}$$
(1)

where ${}^{t+\Delta t}V$ is the volume at time $t+\Delta t$; ${}^{t+\Delta t}\mathcal{R}$ is the virtual work done by external loads; ${}^{t+\Delta t}\tau_{ij}$ is the Cauchy stress tensor at time $t+\Delta t$, and $\delta_{t+\Delta t}e_{ij}$ is the variation in the small strains referred to the configuration at time $t+\Delta t$ [1,2]. Since the configuration at time $t+\Delta t$ is unknown and directly working with increments of Cauchy stresses is unreasonable, this equation cannot be used to derive a beam element. By employing the Green-Lagrange strains and $2^{\rm nd}$ Piola-Kirchhoff stresses, the above principle of virtual work at time $t+\Delta t$ can be replaced by

$$\int_{0}^{t+\Delta t} \sigma_{ij} \delta \int_{0}^{t+\Delta t} \varepsilon_{ij}^{0} dV = {}^{t+\Delta t} \mathscr{R}$$
 (2)

where 0V is the volume at time 0; ${}^{t+\Delta t}\sigma_{ij}$ is the $2^{\rm nd}$ Piola-Kirchhoff stress tensor and ${}^{t+\Delta t}_0\varepsilon_{ij}$ is the Green-Lagrange strain tensor [6]. Equation (2) takes the initial configuration at time 0 as the reference configuration, from which the element formulations can be developed.

2.2. Corotational transformation

In the corotational transformation, when describing displacements and strains at any time point, the reference system is the basic system at the same time point (Fig. 2). The element is formulated in the 6-DOF basic system at this time, then transformed to the global system using the corotational transformation matrix at this time. The transformation matrix is different at different time points because the basic system continuously rotates and translates with the element. The deformational response is considered at the level of the basic coordinate system, whereas the rigid body motion is captured by the transformation matrices relating the basic and global systems. There are 6 DOFs in the basic system because rigid body motion is separated from the deformation and only rotations and an elongation remain in the basic system. In the corotational transformation, the 6x6 element stiffness matrix is derived in the basic system at $t+\Delta t$, then transformed to the global system using the corotational transformation matrix of the current

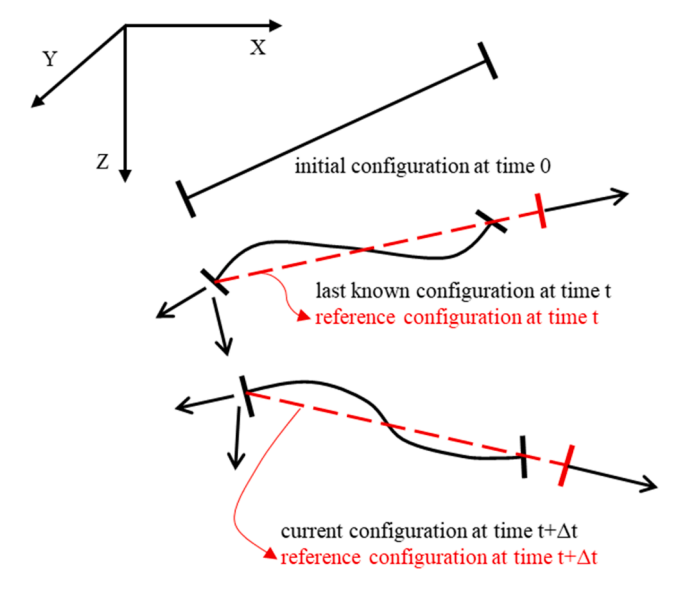


Fig. 2. Illustration of the corotational total Lagrangian formulation (after Mattiasson et al. [7]).

configuration.

The displacements, forces and stiffnesses transformations between the basic and global systems that were implemented in OpenSees are introduced here briefly. The tangential relation between the displacements D_b in the basic system and the displacements \widehat{D} in the global systems can be defined as

$$\delta \mathbf{D}_b = \mathbf{T} \delta \widehat{\mathbf{D}} \tag{3}$$

where T is a transformation matrix connecting the global and basic systems. In geometric linear analysis T is a constant matrix, while in geometric nonlinear analysis T is a function of displacements \widehat{D} . Equating the internal virtual work in both the basic and global systems, the relationship between element end forces in the basic and global systems can be obtained as

$$\widehat{\boldsymbol{P}} = \boldsymbol{T}^T \boldsymbol{P}_b \tag{4}$$

where \hat{P} and P_b are the element end forces at the global system and basic system, respectively. The element tangent stiffness matrix in the global system is obtained from the linearization of Eq. (4), such that

$$\delta \widehat{\boldsymbol{P}} = \delta (\boldsymbol{T}^T \boldsymbol{P}_b) = \boldsymbol{T}^T \delta \boldsymbol{P}_b + \delta \boldsymbol{T}^T \boldsymbol{P}_b = \boldsymbol{T}^T \boldsymbol{K}_b \delta \boldsymbol{D}_b + \delta \boldsymbol{T}^T \boldsymbol{P}_b = (\boldsymbol{T}^T \boldsymbol{K}_b \boldsymbol{T} + \boldsymbol{K}_G) \delta \widehat{\boldsymbol{D}} = \widehat{\boldsymbol{K}} \delta \widehat{\boldsymbol{D}}$$
(5)

where K_b is the tangent stiffness matrix in the basic system, and $\delta P_b = K_b \delta D_b$ is used in the above equation. Here,

$$\widehat{\mathbf{K}} = \mathbf{T}^T \mathbf{K}_h \mathbf{T} + \mathbf{K}_G \tag{6}$$

is the tangent stiffness matrix in the global system. On the right hand side of Eq. (6), the second term K_G is called the external geometric stiffness matrix. The parameterization of 3D finite rotations and detailed derivations of T and K_G are described by Crisfield [5] and de Souza [41]. The element formulation in the basic system is independent to the corotational transformation; therefore, this research uses the current corotational transformation in OpenSees with the element formulation in the basic system modified.

2.3. Corotational total Lagrangian formulation

The corotational total Lagrangian formulation is utilized in the present research to consider geometric nonlinearity in the basic system so that the torsional DOF will be coupled with the axial and flexural DOFs. In the corotational total Lagrangian formulation, the reference configuration is taken as the initial undeformed configuration but translates and rotates in accordance with the motion of the corotating basic system (see Fig. 2). When deriving the stiffness matrix and force recovery in the basic system, we can assume that the basic system is fixed and apply the total Lagrangian formulation in the basic system as shown in Fig. 3. This means that the Green-Lagrange strain tensor, the 2nd Piola-Kirchhoff stress tensor and Eq. (2) will be adopted to describe the element responses with respect to the reference configuration illustrated in Fig. 3.

3. Displacement-based beam element in the basic system

This section presents the development of a new displacement-based beam element in OpenSees, which can be used to simulate the nonlinear behavior of members with asymmetric cross sections. The new displacement-based element can address inelastic behavior through the use of fiber-based cross-section formulations. Small strains, large rotations, and large displacements are assumed in this formulation.

3.1. Coordinate systems of the original OpenSees elements

OpenSees has two coordinate systems: the basic system with 6 DOFs per element, and the global system with 12 DOFs per element. The basic system and global system are represented in Fig. 4. The element ends node I and node J in Fig. 4 are centroids of the cross section. The element stiffness matrix is formulated in the basic system which has the 6 DOFs: one relative axial displacement u_J , two rotations relative to the chord θ_{Iz} and θ_{Jz} , about the z axis, two rotations relative to the chord θ_{Iy} and θ_{Jy} , about the y axis, and one relative angle of twist ϕ_J . Note that OpenSees assumes the cross section is doubly symmetric and all the 6 DOFs are defined with respect to the centroid of the cross section. These relative displacement DOFs in the basic system are the minimum number of geometric variables required to describe the deformation modes of the element in 3D space, which also make sure there are no rigid body modes in the basic system. The six statically independent element end forces corresponding to these displacement DOFs are the axial force N_J , the two bending moments in the xy plane, M_{Iz} and M_{Jz} , the two bending moments in the xz plane, M_{Iy} and M_{Jy} , and the torque T_J . These element end forces and displacements are gathered into vectors

$$\mathbf{D}_b = \begin{bmatrix} u_J & \theta_{Iz} & \theta_{Jz} & \theta_{Iv} & \theta_{Jv} & \phi_{J} \end{bmatrix}^T \tag{7}$$

and

$$\boldsymbol{P}_b = \begin{bmatrix} N_J & M_{Iz} & M_{Jz} & M_{Iy} & M_{Jy} & T_J \end{bmatrix}^T \tag{8}$$

The OpenSees element has 12 DOFs in the global system, i.e., three translational displacements and three rotations at each node. These DOFs are grouped into a vector

$$\widehat{\boldsymbol{D}} = \begin{bmatrix} \boldsymbol{U}_{I}^{T} & \boldsymbol{\gamma}_{I}^{T} & \boldsymbol{U}_{I}^{T} & \boldsymbol{\gamma}_{I}^{T} \end{bmatrix}^{T}$$

$$(9)$$

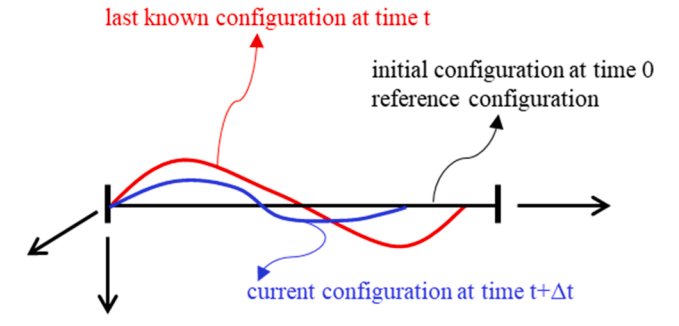


Fig. 3. Total Lagrangian method in the basic system.

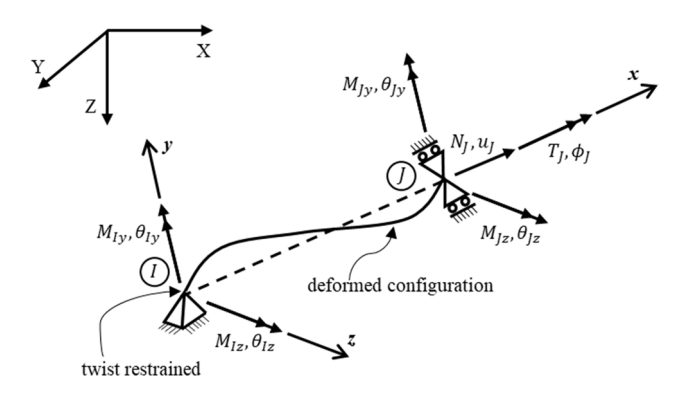


Fig. 4. Basic and global coordinate systems in space (after de Souza [41]).

where U_I^T and U_J^T are 3x1 vectors with the translational displacements, and γ_I^T and γ_J^T are 3x1 pseudo-vectors that define the rotations of nodes I and J, respectively. In the absolute sense, these rotations can be arbitrarily large, although it is assumed that the relative rotation of two element ends is small. As such, the OpenSees element can experience finite displacements and rigid body rotations; however, the deformations along the element are considered to be moderate. The corresponding work conjugate forces in the global system are

3.2. Coordinate systems for asymmetric sections

Since the new element is implemented in the OpenSees corotational framework, the original OpenSees coordinate systems described in Section 3.1 are adopted with some modifications for the basic coordinate system. The same global system with the original OpenSees element is used here; however, due to the noncoincident shear center and centroid of the beam element with asymmetric sections, its basic system is slightly different as shown in Fig. 5. The modified basic system is defined by two set of coordinates: x, y, z and x, y, z. The coordinate system x, y, z is chosen such that x passes through the end cross-section centroids C and C', and y and z are the section principal axes. A parallel set of coordinates x, y, z is chosen such that x passes through the end cross-section shear centers S and S', and y and z are parallel to the principal y and z axes of the cross section. Let v and w denote the displacements of the shear center in the y and z directions, u the axial displacement along the centroidal axis CC', and ϕ the angle of twist

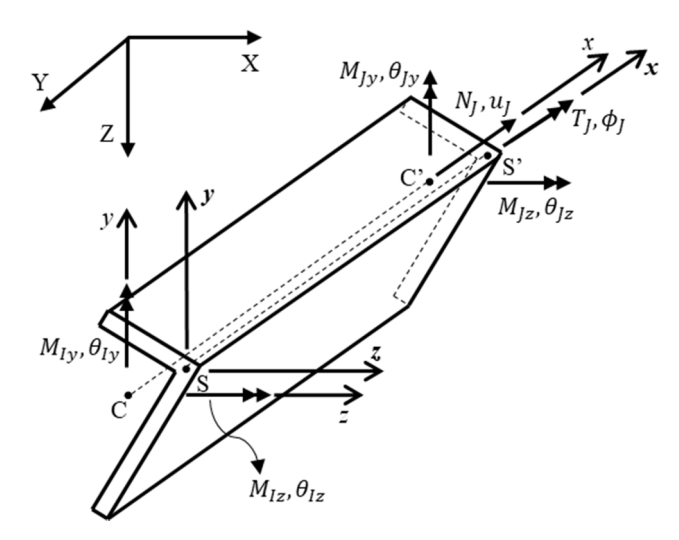


Fig. 5. Basic and global coordinate systems in space for asymmetric sections.

about the shear center axis SS'. Such a coordinate system will uncouple displacements and rotations in the sense of the first order effect [22,23].

The element stiffness matrix is formulated in the basic system with the 6 DOFs presented in Eqs. (7) and (8). However, the definitions of the DOFs are different as follows: one relative axial displacement u_J of the centroids, two rotations relative to the chord θ_{Iz} and θ_{Jz} , about the z axis, two rotations relative to the chord θ_{Iy} and θ_{Jy} , about the y axis, and one relative angle of twist ϕ_J about the x axis. The six statically independent element end forces corresponding to these displacements are: the axial force N_J acting along the centroidal axis CC'; the two bending moments acting about the principle axis z and in the xy plane, M_{Iz} and M_{Jz} ; the two bending moments acting about the principle axis y and in the y plane, y and y and y and y and the torsional moment y about the shear center axis SS' [42].

Following the corotational transformation procedure, the forces, displacements and stiffness matrix need to be transformed to the global system. However, in the current definition of the basic system, some DOFs are defined with respect to the centroid, while others are defined with respect to the shear center, which makes the corotational transformation cannot be applied directly [34]. Consequently, all DOFs (end forces and displacements) need to be transformed to one reference point in advance of the corotational transformation. Note that in the basic system, the axial force is referred to the centroid, the shear forces and torque are defined with respect to the shear center, and the moments act in the planes containing the shear center. Thus, it is straightforward to transform all DOFs to the shear center, because only the axial force needs to be transformed. If other points (e.g., the centroid) are selected as the reference point, the shear forces need to be transformed, which is more difficult because the shear forces are only recovered after the corotational transformation. Therefore, it is proper to choose the shear center as the reference point and the shear center axis as the member reference axis before the corotational transformation. The coordinate system x, y, z is referred as the element basic reference system with the element end forces P_r and displacements D_r act through the shear center. The following equations are used to transform all DOFs to the shear center

$$P_r = T_r^T P_b \tag{11}$$

$$D_b = T_r D_r \tag{12}$$

where the cross-section transformation matrix is [34]

$$\boldsymbol{T}_{r}^{T} = \begin{bmatrix} 1 & 0 & 0 & 0 & 0 & 0 \\ y_{s} & 1 & 0 & 0 & 0 & 0 \\ -y_{s} & 0 & 1 & 0 & 0 & 0 \\ -z_{s} & 0 & 0 & 1 & 0 & 0 \\ z_{s} & 0 & 0 & 0 & 1 & 0 \\ 0 & 0 & 0 & 0 & 0 & 1 \end{bmatrix}$$

$$(13)$$

and y_s and z_s are coordinates of the shear center relative to the centroid. Consequently, the stiffness matrix in the element basic reference system is

$$\mathbf{K}_r = \mathbf{T}_r^T \mathbf{K}_b \mathbf{T}_r \tag{14}$$

With this consideration, the coordinate system x, y, z in Fig. 5 is the same with the basic system in Fig. 4 in the sense of corotational transformation, but the displacement and force DOFs should be replaced by D_r and P_r . The corotational transformation will remain the same as in the original OpenSees with the Eqs. (3), (4) and (6) being modified as

$$\delta D_r = T \delta \hat{D} \tag{15}$$

$$\widehat{\boldsymbol{P}} = \boldsymbol{T}^T \boldsymbol{P}_r \tag{16}$$

$$\widehat{K} = T^T K_r T + K_G \tag{17}$$

3.3. Beam section kinematics

With the commonly used kinematic assumption of the Euler-Bernoulli beam theory and disregarding the in-plane distortion behavior of the cross section, the motion of a material point P (x, y, z) (P is expressed in the coordinate system x, y, z shown in Fig. 5) in the beam section is expressed in terms of the displacement components [43,44]

$$u_p = u - yv' - zw' + z\phi v' - y\phi w'$$

$$v_p = v - \phi(z - z_s)$$

$$w_p = w + \phi(y - y_s) \tag{18}$$

where y_s and z_s are defined in Eq. (13); in addition, u, v, w and ϕ are defined in Section 3.2. In the derivation of Eq. (18), small rotation assumptions are enforced, which is appropriate since the corotational transformation addresses the rigid body motions. The nonlinear contributions in u_p are used to consider the combined effects of torsion and bending. The longitudinal/axial component of the Green-Lagrange strain is expressed as

$$\varepsilon = \frac{\partial u_p}{\partial x} + \frac{1}{2} \left(\frac{\partial u_p}{\partial x} \right)^2 + \frac{1}{2} \left(\frac{\partial v_p}{\partial x} \right)^2 + \frac{1}{2} \left(\frac{\partial w_p}{\partial x} \right)^2 \tag{19}$$

The high-order term $\frac{1}{2}(\partial u_p/\partial x)^2$ is negligible compared to $\partial u_p/\partial x$ because it is assumed that the term $\partial u_p/\partial x$ is small compared to unity. Hence, the Green-Lagrange strain becomes

$$\varepsilon = \frac{\partial u_p}{\partial x} + \frac{1}{2} \left(\frac{\partial v_p}{\partial x} \right)^2 + \frac{1}{2} \left(\frac{\partial w_p}{\partial x} \right)^2 \tag{20}$$

Taking derivatives of the displacement field in Eq. (18) with respect to x and substituting the results into Eq. (20) gives

$$\varepsilon = u' - yv'' - zw'' + \frac{1}{2} [(v')^2 + (w')^2] + \frac{1}{2} [(y - y_s)^2 + (z - z_s)^2] (\phi')^2 + (z_s v' - y_s w') \phi' + (zv'' - yw'') \phi$$
(21)

Compared with the strain term $\varepsilon=u^{'}-yv^{''}-zw^{''}$ used for the original OpenSees displacement-based element, Eq. (21) has the following extra terms

$$\begin{array}{ll} \frac{1}{2} \left[(\vec{v} \)^2 + (\vec{w} \)^2 \right] & \text{: geometric nonlinear term (coupling between the axial tension/compression and bending)} \\ \frac{1}{2} \left[\left(y - y_s \right)^2 + (z - z_s)^2 \right] (\vec{\phi} \)^2 & \text{: Wagner term (coupling between the axial strain and torsion)} \\ (z_s \vec{v} - y_s \vec{w} \) \vec{\phi} + (z \vec{v} \ - y_s \vec{w} \) \vec{\phi} & \text{: coupling term between bending and torsion (effect of this coupling on the axial strain)} \\ \end{array}$$

The shear strain at P resulting from uniform twisting ϕ of a thin-walled open section member is approximated by [21]

$$\gamma = 2n\phi' \tag{22}$$

in which n is the perpendicular distance of point P (x, y, z) from the midthickness line of the cross section. Shear strains due to bending are neglected.

3.4. Displacement-based element formulation

In this section, the element governing equilibrium equation is derived from the principle of virtual work with the aid of the kinematic assumptions and the displacement shape functions. Linearization of the governing equation leads to the element tangent stiffness and the equation for force recovery. To start, the axial strain and shear strain can be put together in vector form as

$$\epsilon = \begin{bmatrix} \varepsilon \\ \gamma \end{bmatrix}$$
(23)

The terms in the strain vector can be expressed in matrix form as

$$\epsilon = Yd$$
 (24)

where

$$Y = \begin{bmatrix} 1 & -y & z & (y - y_s)^2 + (z - z_s)^2 & 0 \\ 0 & 0 & 0 & 0 & 2n \end{bmatrix}$$
 (25)

and

$$d = \begin{bmatrix} u' + \frac{1}{2} [(v')^2 + (w')^2] + (z_s v' - y_s w') \phi' \\ v'' + w'' \phi \\ -w'' + v'' \phi \\ \frac{1}{2} (\phi')^2 \\ \phi' \end{bmatrix}$$
(26)

Vector \boldsymbol{d} is the section deformation vector. Matrix \boldsymbol{Y} relates strains on a material point and the section deformations on the corresponding section. The variation of the strain vector is obtained as

$$\delta \epsilon = Y \delta d \tag{27}$$

in which

$$\delta d = \begin{bmatrix} \delta u' + v' \delta v' + w' \delta w' + (z_s \delta v' - y_s \delta w') \phi' + (z_s v' - y_s w') \delta \phi' \\ \delta v'' + \phi \delta w'' + w'' \delta \phi \\ -\delta w'' + \phi \delta v'' + v'' \delta \phi \\ \phi' \delta \phi \\ \delta \phi' \end{cases}$$
(28)

And δd can be expressed as

$$\delta d = N_{\delta d1} \delta v \tag{29}$$

where

$$N_{\delta d1} = \begin{bmatrix} 1 & v' + z_s \phi & w' - y_s \phi & 0 & 0 & 0 & z_s v' - y_s w' \\ 0 & 0 & 0 & 1 & \phi & w' & 0 \\ 0 & 0 & 0 & \phi & -1 & v' & 0 \\ 0 & 0 & 0 & 0 & 0 & 0 & \phi \\ 0 & 0 & 0 & 0 & 0 & 0 & 1 \end{bmatrix}$$
(30)

$$\delta \mathbf{v} = \begin{bmatrix} \delta u' & \delta v' & \delta w' & \delta v'' & \delta w'' & \delta \phi & \delta \phi' \end{bmatrix}^T \tag{31}$$

Thus, Eq. (27) becomes

$$\delta \epsilon = Y N_{\delta d1} \delta v \tag{32}$$

In the basic system, the axial elongation field, the transverse displacement field and the twist displacement field along the element can be interpolated between the element DOFs with the help of shape functions

$$u = \boldsymbol{N}_{u}^{T} \boldsymbol{D}_{b} = [N_{u1} \quad 0 \quad 0 \quad 0 \quad 0 \quad 0] \boldsymbol{D}_{b}$$

$$v = \boldsymbol{N}_{v}^{T} \boldsymbol{D}_{b} = [0 \quad N_{v1} \quad N_{v2} \quad 0 \quad 0 \quad 0] \boldsymbol{D}_{b}$$

$$w = \boldsymbol{N}_{w}^{T} \boldsymbol{D}_{b} = [0 \quad 0 \quad 0 \quad N_{w1} \quad N_{w2} \quad 0] \boldsymbol{D}_{b}$$

$$\phi = \mathbf{N}_{\boldsymbol{a}}^{T} \mathbf{D}_{\boldsymbol{b}} = \begin{bmatrix} 0 & 0 & 0 & 0 & N_{\phi 1} \end{bmatrix} \mathbf{D}_{\boldsymbol{b}}$$
(33)

The shape functions in Eq. (33) are chosen as follows: cubic Hermitian functions for the transverse displacements, and a linear function for

the axial deformation and twist. Specifically, the shape functions utilized in the current development are

$$N_{u1}=N_{\phi 1}=\frac{x}{l_0}$$

$$N_{v1} = -N_{w1} = x \left(1 - \frac{x}{l_0}\right)^2$$

$$N_{v2} = -N_{w2} = x \left(\frac{x}{l_0}\right) \left(\frac{x}{l_0} - 1\right) \tag{34}$$

where l_0 is the length of the undeformed element. With the help of shape functions, δv can be written in terms of the element DOFs, as shown

$$\delta v = N_{\delta d2} \delta D_b \tag{35}$$

in which

$$N_{\delta d2} = \begin{pmatrix} N_{u1}^{'} & 0 & 0 & 0 & 0 & 0 \\ 0 & N_{v1}^{'} & N_{v2}^{'} & 0 & 0 & 0 \\ 0 & 0 & 0 & N_{w1}^{'} & N_{w2}^{'} & 0 \\ 0 & N_{v1}^{''} & N_{v2}^{''} & 0 & 0 & 0 \\ 0 & 0 & 0 & N_{w1}^{''} & N_{w2}^{''} & 0 \\ 0 & 0 & 0 & 0 & 0 & N_{\phi 1} \\ 0 & 0 & 0 & 0 & 0 & N_{\phi 1}^{'} \end{pmatrix}$$

$$(36)$$

Therefore, Eq. (32) becomes

$$\delta \epsilon = Y N_{\delta d1} N_{\delta d2} \delta \mathbf{D}_b \tag{37}$$

Here, the Total Lagrangian formulation is used for the virtual work principle. In the basic system, the stresses and strains are referred to the undeformed configuration of the beam element. The principle of virtual work can be written in a general form as

$$\int_{V_0} \delta \epsilon^T \boldsymbol{\sigma} dV - \delta \boldsymbol{D}_b^T \boldsymbol{P}_{ext} = 0$$
(38)

where $\sigma = \begin{bmatrix} \sigma & \tau \end{bmatrix}^T$ is the corresponding stress vector, V_0 is the volume of the undeformed element, and P_{ext} is a vector of external forces. After substituting Eq. (37) into Eq. (38) and rearranging, we have

$$\delta \boldsymbol{D}_{b}^{T} \left\{ \int_{l_{0}} \boldsymbol{N}_{\delta d2}^{T} \boldsymbol{N}_{\delta d1}^{T} \left(\int_{A_{0}} \boldsymbol{Y}^{T} \boldsymbol{\sigma} dA \right) dx - \boldsymbol{P}_{ext} \right\} = 0$$
(39)

and

$$\delta \mathbf{D}_{b}^{T} \left\{ \int_{l_{0}} N_{\delta d2}^{T} N_{\delta d1}^{T} \mathbf{S} dx - \mathbf{P}_{ext} \right\} = 0$$

$$(40)$$

where A_0 is the cross-section area of the undeformed element; and S is the vector of section forces expressed as

$$S = \int_{A_0} \mathbf{Y}^T \boldsymbol{\sigma} dA = \begin{bmatrix} \int_{A_0} \boldsymbol{\sigma} dA \\ -\int_{A_0} \boldsymbol{y} \boldsymbol{\sigma} dA \\ \int_{A_0} \boldsymbol{z} \boldsymbol{\sigma} dA \\ \int_{A_0} \left[(\boldsymbol{y} - \boldsymbol{y}_s)^2 + (\boldsymbol{z} - \boldsymbol{z}_s)^2 \right] \boldsymbol{\sigma} dA \end{bmatrix} = \begin{bmatrix} N \\ M_z \\ M_y \\ W \\ T \end{bmatrix}$$

$$(41)$$

where N is the axial force, M_z is the bending moment about the z-axis, M_y is the bending moment about the y-axis, W is the Wagner stress resultant, and T is the St. Venant torque. The governing equilibrium equation can be rewritten as

$$\mathbf{g} = \int_{b_0} \mathbf{N}_{\delta d1}^T \mathbf{N}_{\delta d1}^T \mathbf{S} dx - \mathbf{P}_{ext} = 0 \tag{42}$$

The governing equation is in general a nonlinear function of the unknown displacement increment. It should be linearized to obtain the element tangent stiffness matrix. Such a linearization process can be achieved by expanding the governing equation at $(i+1)^{th}$ iteration based on previous configuration at i^{th} iteration. The details of the linearization process are shown in Appendix A, from which the following iteration equation can be obtained

$$\mathbf{K}_{b}\Delta\mathbf{D}_{b} = \mathbf{P}_{ext}^{i+1} - \mathbf{P}_{int}^{i} \tag{43}$$

where

$$\mathbf{K}_{b} = \int_{I_0} \mathbf{N}_{\delta d2}^T \mathbf{G} \mathbf{N}_{\delta d2} dx + \int_{I_0} \mathbf{N}_{\delta d2}^T \mathbf{N}_{\delta d1}^T \mathbf{K}_{\delta} \mathbf{N}_{\delta d1} \mathbf{N}_{\delta d2} dx \tag{44}$$

$$P_{int}^{i} = \int_{l_0} N_{\delta d2}^{T} N_{\delta d1}^{T} S^{i} dx \tag{45}$$

$$\mathbf{P}_{ext}^{i+1} = \mathbf{P}_{ext}^{i} + \Delta \mathbf{P}_{ext} \tag{46}$$

 K_b is the element tangent stiffness matrix in the basic system, the first integral in which is the element internal geometric stiffness matrix and the second integral is the element material stiffness matrix. The definition of the auxiliary matrix G and the section stiffness matrix K_s can be found in Appendix A. In addition, P_{ext}^{i+1} and P_{int}^{i} are the external load vector in $(i+1)^{th}$ iteration and the element internal resisting forces in i^{th} iteration, respectively. The vector S^i represents section forces in i^{th} iteration.

3.5. Fiber section and material nonlinearity

In order to consider material nonlinearity, the beam section is discretized into a set of fibers so that the section stiffness matrix K_s can be obtained through numerical integration. In this element, it is assumed that the uniform torsion behavior is linear elastic so that shear strain is always elastic, and GJ is used as the rigidity of uniform torsion. Thus, the uniaxial constitutive law is used to check the yielding of the material. Note that the tangent Young's modulus E can be updated for each fiber as it reaches plastic stage. The calculation of K_s through numerical integration is shown as

$$K_{s} = \begin{bmatrix} \sum_{j=1}^{n_{1}} E_{j}A_{j} & -\sum_{j=1}^{n_{1}} y_{j}E_{j}A_{j} & \sum_{j=1}^{n_{1}} z_{j}E_{j}A_{j} & \sum_{j=1}^{n_{1}} p_{j}^{2}E_{j}A_{j} & 0 \\ -\sum_{j=1}^{n_{1}} y_{j}E_{j}A_{j} & \sum_{j=1}^{n_{1}} y_{j}^{2}E_{j}A_{j} & -\sum_{j=1}^{n_{1}} y_{j}z_{j}E_{j}A_{j} & -\sum_{j=1}^{n_{1}} p_{j}^{2}y_{j}E_{j}A_{j} & 0 \\ \sum_{j=1}^{n_{1}} z_{j}E_{j}A_{j} & -\sum_{j=1}^{n_{1}} y_{j}z_{j}E_{j}A_{j} & \sum_{j=1}^{n_{1}} z_{j}^{2}E_{j}A_{j} & \sum_{j=1}^{n_{1}} p_{j}^{2}z_{j}E_{j}A_{j} & 0 \\ \sum_{j=1}^{n_{1}} p_{j}^{2}E_{j}A_{j} & -\sum_{j=1}^{n_{1}} p_{j}^{2}y_{j}E_{j}A_{j} & \sum_{j=1}^{n_{1}} p_{j}^{2}z_{j}E_{j}A_{j} & 0 \\ 0 & 0 & 0 & GJ \end{bmatrix}$$

$$0 \qquad 0 \qquad 0 \qquad 0 \qquad 0 \qquad 0$$

$$\delta \in = \begin{pmatrix} \lambda_{1} & \lambda_{2} & \lambda_{1} & \lambda_{2} & \lambda_{2} & \lambda_{1} & \lambda_{2} & \lambda_$$

where E_j , A_j , y_j , and z_j and p_j are the tangent Young's modulus, area, y coordinate, z coordinate and p value (see Eq. (A.8) in Appendix A for

definition) of the j^{th} fiber, respectively; n_1 is the number of fibers on the section. Similarly, the section forces can be calculated numerically as shown in Eq. (48). Here the torque due to uniform torsion is achieved directly from the first derivative of the twist rotation ϕ and the equivalent section torsional rigidity GJ because of the assumption of linear elastic St. Venant torsional behavior. Note that the nonlinear torsional behavior is considered through including the Wanger stress resultant W [45].

$$S = \begin{bmatrix} \sum_{j=1}^{n_1} \sigma_j A_j \\ -\sum_{j=1}^{n_1} y_j \sigma_j A_j \\ \sum_{j=1}^{n_1} z_j \sigma_j A_j \\ \sum_{j=1}^{n_1} \left[(y_j - y_s)^2 + (z_j - z_s)^2 \right] \sigma_j A_j \\ GJ\phi \end{bmatrix}$$
(48)

Thus, the matrix G in Eq. (44) can be obtained from results of the numerical calculation of section forces S. Numerical integration methods like Gaussian quadrature are used to calculate K_b and P_{int}^i .

3.6. Membrane locking

In order to avoid membrane locking, as recommended by Crisfield [4,5,43], the high order term $\frac{1}{2}\left[(v^{\cdot})^2+(w^{\cdot})^2\right]$ in Eq. (21) can be replaced by an effective membrane strain $\frac{1}{l_0}\int_0^{l_0}\frac{1}{2}\left[(v^{\cdot})^2+(w^{\cdot})^2\right]dx$. This integral can be obtained by assuming cubic shape functions for v and w; thus, Eq. (21) should be substituted by

$$\varepsilon = u' - yv'' - zw'' + \frac{1}{60}\theta_b^T X \theta_b + \frac{1}{2} \left[(y - y_s)^2 + (z - z_s)^2 \right] (\phi')^2 + (z_s v' - y_s w') \phi' + (zv'' - yw'') \phi$$
(49)

in which the vector $\boldsymbol{\theta}_b = \begin{bmatrix} \theta_{Iz} & \theta_{Iy} & \theta_{Jz} & \theta_{Jy} \end{bmatrix}^T$ holds the local slopes in the basic system, and the matrix \boldsymbol{X} is defined as

$$X = \begin{bmatrix} 4 & 0 & -1 & 0 \\ 0 & 4 & 0 & -1 \\ -1 & 0 & 4 & 0 \\ 0 & -1 & 0 & 4 \end{bmatrix}$$
 (50)

Thus, the modified d is

$$\mathbf{d} = \begin{bmatrix} u' + \frac{1}{60} \boldsymbol{\theta}_b^T \mathbf{X} \boldsymbol{\theta}_b + (z_s v' - y_s w') \boldsymbol{\phi}' \\ v'' + w'' \boldsymbol{\phi} \\ -w'' + v'' \boldsymbol{\phi} \\ \frac{1}{2} (\boldsymbol{\phi}')^2 \\ \boldsymbol{\phi}' \end{bmatrix}$$
 (51)

The variation of strain vector is obtained as

$$\delta \epsilon = Y \delta d \tag{52}$$

in which

$$\delta \boldsymbol{d} = \begin{bmatrix} \delta u' + \frac{1}{30} \boldsymbol{\theta}_b^T \boldsymbol{X} \delta \boldsymbol{\theta}_b + (z_s \delta v' - y_s \delta w') \boldsymbol{\phi}' + (z_s v' - y_s w') \delta \boldsymbol{\phi}' \\ \delta v'' + \boldsymbol{\phi} \delta w'' + w'' \delta \boldsymbol{\phi} \\ -\delta w'' + \boldsymbol{\phi} \delta v'' + v'' \delta \boldsymbol{\phi} \\ \boldsymbol{\phi}' \delta \boldsymbol{\phi}' \\ \delta \boldsymbol{\phi}' \end{bmatrix}$$

$$(53)$$

And δd can be expressed as

$$\delta d = N_{\delta d1} \delta v \tag{54}$$

where

$$\delta \mathbf{v} = \begin{bmatrix} \delta u' & \delta \theta_{Iz} & \delta \theta_{Iy} & \delta \theta_{Jz} & \delta \theta_{Jy} & \delta v' & \delta w' & \delta v'' & \delta w'' & \delta \phi & \delta \phi' \end{bmatrix}^T$$
(56)

So

for the matrix \boldsymbol{G} that takes the following form

$$\delta \epsilon = Y N_{\delta d1} \delta v \tag{57}$$

with the aid of shape functions, δv can be written in terms of the element DOFs

$$\delta v = N_{\delta d2} \delta D_b \tag{58}$$

in which $N_{\delta d2}$ is rederived as

$$N_{\delta d2} = \begin{bmatrix} N_{u1}^{'} & 0 & 0 & 0 & 0 & 0 & 0 \\ 0 & 1 & 0 & 0 & 0 & 0 & 0 \\ 0 & 0 & 0 & 1 & 0 & 0 & 0 \\ 0 & 0 & 1 & 0 & 0 & 0 & 0 \\ 0 & 0 & 1 & 0 & 0 & 0 & 0 \\ 0 & 0 & 0 & 0 & 1 & 0 & 0 \\ 0 & N_{v1}^{'} & N_{v2}^{'} & 0 & 0 & 0 & 0 \\ 0 & 0 & 0 & N_{w1}^{'} & N_{w2}^{'} & 0 & 0 \\ 0 & N_{v1}^{'} & N_{v2}^{''} & 0 & 0 & 0 & 0 \\ 0 & 0 & 0 & N_{w1}^{''} & N_{w2}^{''} & 0 & 0 \\ 0 & 0 & 0 & 0 & N_{w1}^{''} & N_{w2}^{''} & 0 \\ 0 & 0 & 0 & 0 & 0 & N_{\phi 1}^{'} \\ 0 & 0 & 0 & 0 & 0 & N_{\phi 1}^{'} \end{bmatrix}$$

$$(59)$$

Therefore, Eq. (57) becomes

$$\delta \epsilon = Y N_{\delta d1} N_{\delta d2} \delta D_b \tag{60}$$

The same linearization process for Eq. (42) is adopted as in Appendix A with the new matrices $N_{\delta d1}$ and $N_{\delta d2}$ in the present section. The same element formulation (Eqs. (43)-(46)) is obtained and the only change is

3.7. Rigid offsets

Generally, thin-walled asymmetric members are connected eccentrically and sometimes structural joints should be considered as being of a finite size. Therefore, the element reference ends should be offset to the connecting point from the shear center, as shown in Fig. 6. Nodes I and J are shear centers, while nodes 1 and 2 are the connecting points of the element (element reference ends). Here, d_{XI} , d_{YI} and d_{ZI} are the offsets specified with respect to the global coordinate system for element end node I, and they are designated to be the coordinates of node I minus the coordinates of node 1. Similarly, d_{XJ} , d_{YJ} and d_{ZJ} are the coordinates of node I minus the coordinates of node 2.

This phenomenon can be considered systematically by utilizing a transformation matrix to model the rigid offsets [26,28,46]. The relationship between end forces of the element reference ends (1 and 2 in Fig. 6) and the shear centers (I and J in Fig. 6) can be derived with the help of equilibriums of rigid offsets. The details of this transformation are shown in Appendix B.

3.8. Element state determination

The following algorithm is utilized for element state determination of the displacement-based element. Once the incremental displacements and rotations are retrieved from the global solution, the element state determination process is as follows

- 1. Update the nodal translational displacements and rotations in the global system.
- 2. Compute the rotations and the axial displacement in the basic system through corotational transformation.

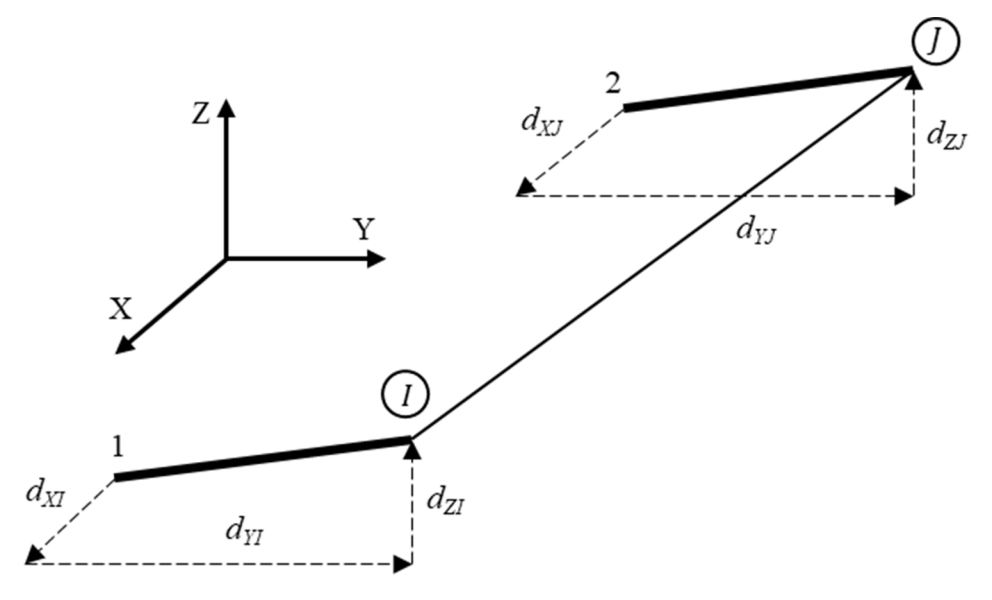


Fig. 6. Element with rigid offsets.

- 3. Compute axial strain at each fiber according to Eq. (24), and then update the stresses and fiber stiffnesses through constitutive models.
- 4. Compute section stiffnesses and forces according to Eqs. (47) and (48) using the updated stresses and fiber stiffnesses through numerical integration across each section. Note that the torsional rigidity and the St. Venant torque are calculate separately from the section numerical integration.
- 5. Compute the element tangent stiffness matrix and the internal force vector in the basic system according to Eqs. (44) and (45).
- Compute the global tangent stiffness matrix and global internal force vector through corotational transformation according to Eqs. (4) and (6). The transformation in Appendix B should be applied if rigid offsets need to be included.
- 7. Conduct the convergence test. If the residual is smaller than the threshold, then commence the next increment. Otherwise go back to step 1 and continue the iteration.

4. Validation of formulation

Eleven examples are shown here to validate the accuracy of this new element. In examples 1–4 and 6–8, the material is assumed to be linear elastic. Examples 5, 9, 10 and 11 address both elastic and inelastic materials. These validations show that the new element can simulate both geometric and material nonlinearity accurately. In the following, "DBxx" means using xx number of the new displacement-based elements with membrane locking remedied; while "DBxx-with locking" means

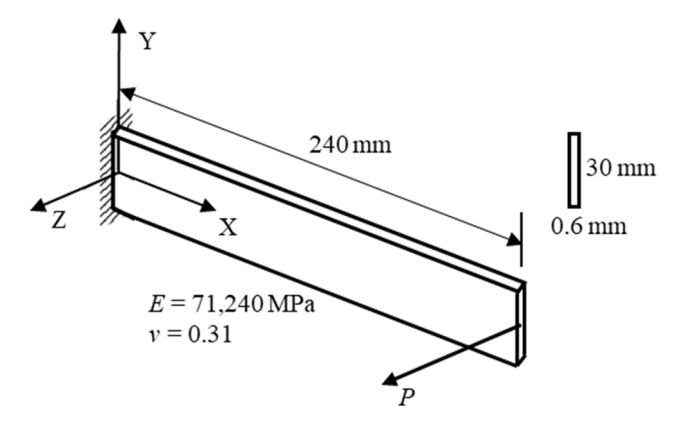


Fig. 7. Inextensional bending of a cantilever.

using xx number of the new displacement-based element elements with membrane locking.

4.1. Inextensional bending

This example compares the simulations of inextensional bending of a cantilever (see Fig. 7) using the original OpenSees displacement-based element (which is appropriate only for symmetric cross sections) [35], the new element with membrane locking, and the new element with membrane locking remedied. Through this example, the accuracy of the element with membrane locking remedied is validated. When a beam element cannot bend without stretching, the energy is incorrectly shifted to membrane energy, resulting in underprediction of displacements and strains. In this structure, a concentrated lateral force P in the global Z direction is applied to the tip of the cantilever.

Fig. 8 compares the force–displacement relationship using the original OpenSees element and the new element with membrane locking. With the increase of elements, both results converge to the same answer. However, the new element with membrane locking converges too slowly compared with the original OpenSees element. As seen in Figs. 8, 5

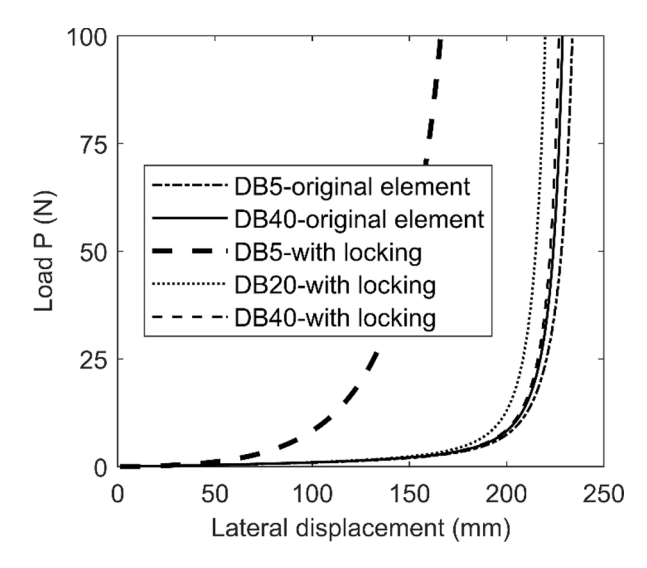


Fig. 8. Comparison of original OpenSees element and new element with membrane locking.

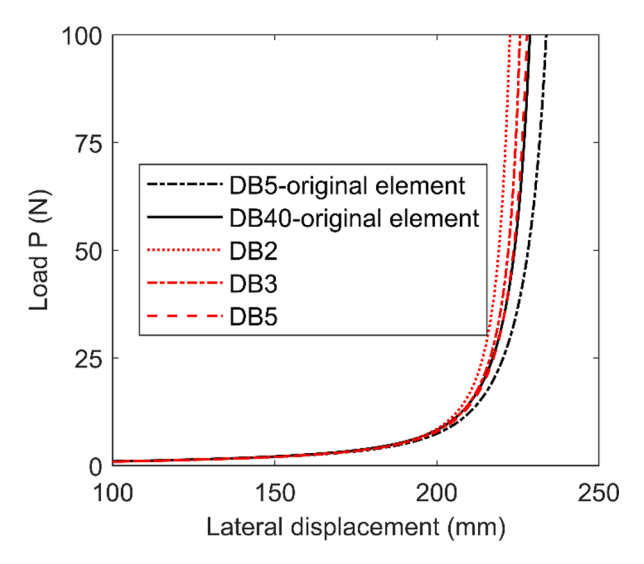


Fig. 9. Comparison of original OpenSees element and new element with membrane locking remedied.

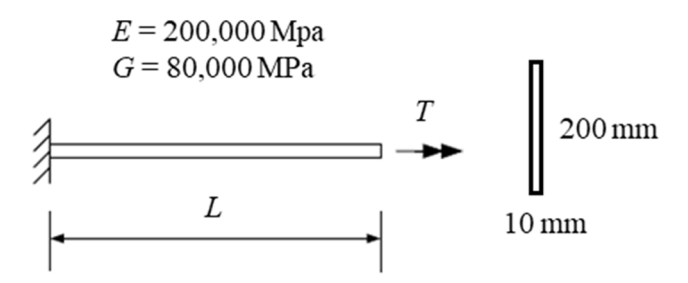


Fig. 10. Nonlinear torsion of a cantilever.

original OpenSees elements and 20 new elements with membrane locking can have comparable accuracy. Fig. 9 shows the results of the new element with membrane locking remedied. It can be seen that when membrane locking is alleviated, the new element can give more accurate answers compared with the original OpenSees element. Five new elements with membrane locking remedied are enough to simulate this phenomenon.

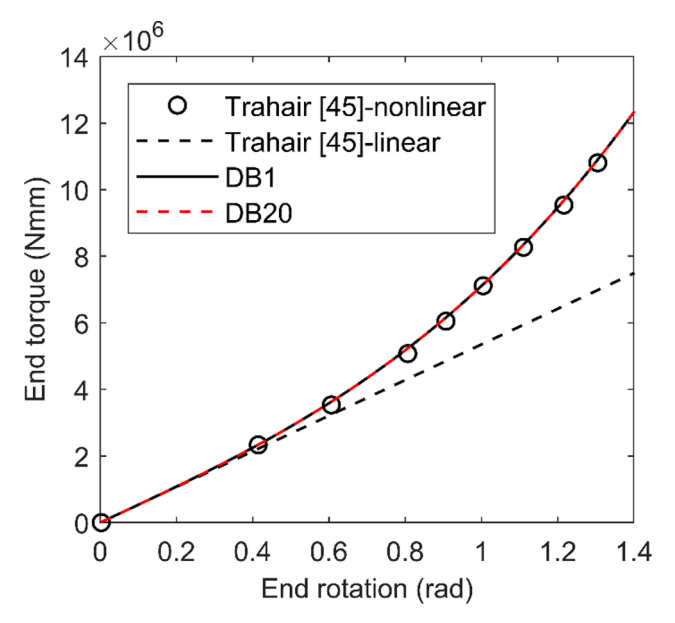


Fig. 11. Moment end-rotation relationship for nonlinear torsion.

4.2. Nonlinear torsion

This example considers a cantilever beam of rectangular cross section (see Fig. 10) subjected to end torque T. The size of the rectangular cross section is 200×10 mm. The beam properties are Young's modulus E=200,000 MPa and G=80,000 MPa, and length L=1,000 mm. The results obtained using 1 and 20 new elements are shown in Fig. 11 and compared with the theoretical solution of Trahair [45]. It is shown that the new element can consider the Wagner effect, which induced the nonlinear phenomenon. The cantilever has axial shortening deformation due to the applied torque. Since the results of using 20 displacement-based elements coincide with the results of using 1 element, it can be accepted that only 1 element is enough to model the nonlinear torsion behavior by adopting the newly developed displacement-based element. In addition, Battini and Pacoste [31] also presented a similar example of nonlinear torsion of a rectangular section, where 20 elements were used to get the results in their work.

4.3. Torsion of a cantilever beam with an angle section

This example considers a cantilever beam with an angle section subjected to an end torque acting on its shear center. As shown in Fig. 12, the geometric and material properties of the cantilever are: $L=177.8~\mathrm{mm}$, $\alpha=90^\circ$, $b=14.605~\mathrm{mm}$, $t=0.9601~\mathrm{mm}$, Young's modulus $E=89,632~\mathrm{MPa}$ and shear modulus $G=33,445~\mathrm{MPa}$. The example was experimentally and numerically studied by different researchers [29,47]. Fig. 13 compares the path of shear center B of the end cross section obtained by the present study, the experimental results from Gregory [47], and the numerical results from Hsiao and Lin [29] using 20 elastic beam elements. This work uses 20 displacement-based elements, whose results match with the experimental and numerical results very well.

4.4. Flexural-torsional interaction

This example investigates the influence of bending moments on the torsional stiffness of a simply supported beam. The experiments were conducted by Engel and Goodier [48] on simply supported angle bars (see Fig. 14). The material was 61 S-T aluminum with Young's modulus E=10,000 ksi and shear modulus G=3,750 ksi. The properties of the monosymmetric angle section are: L=36.8 in., $\alpha=90^{\circ}$, b=1 in., and t=0.030 in. Bending moments acting in the plane of symmetry were applied to the ends of the angle bar to produce constant bending moment between supports. A torque is applied to the mid-span of the member. Fig. 15 shows the comparison of torque-twist lines from

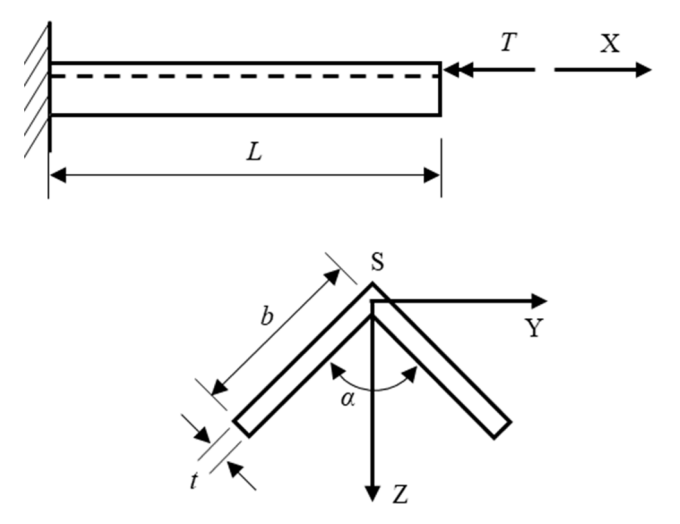


Fig. 12. Torsion of a cantilever beam of angle section.

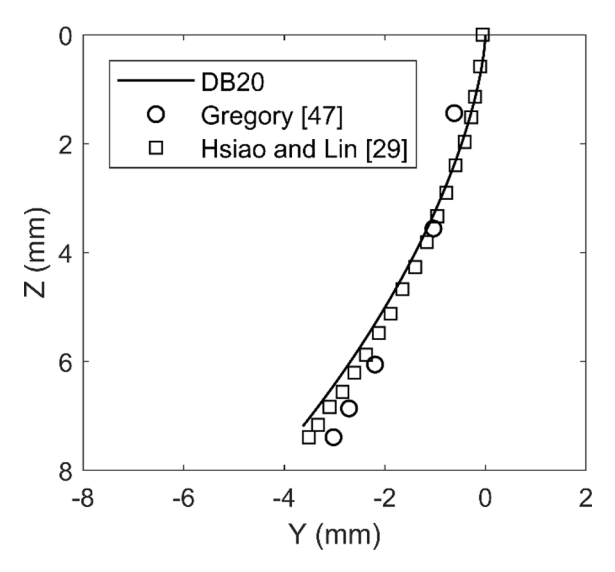


Fig. 13. Path of point B during torsional behavior.

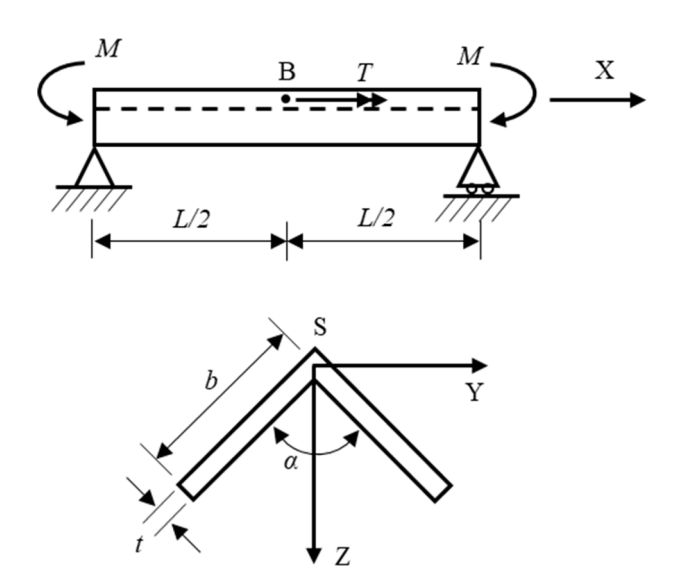


Fig. 14. Simply supported angle bar subjected to end moments and mid-span torque.

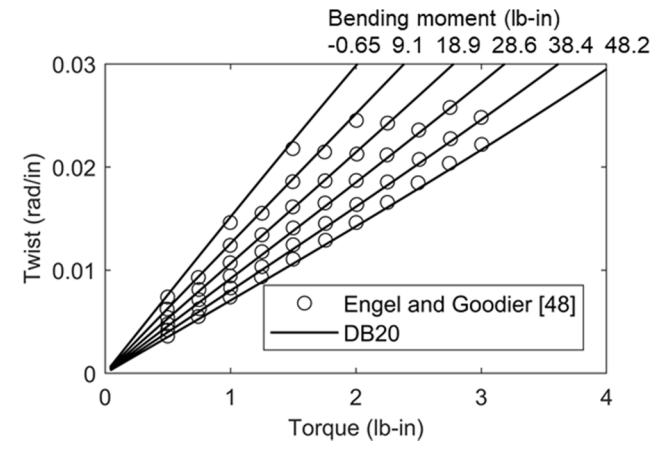


Fig. 15. Twist per unit length versus applied.

experiments and simulations using 20 elements in the present study. The

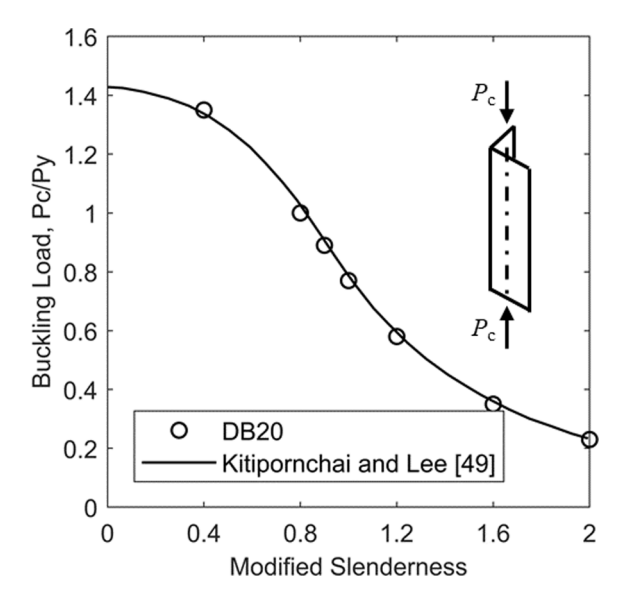


Fig. 16. Flexural-torsional buckling of concentrically loaded angle struts (elastic).

results indicate that the new element can successfully model the flexural-torsional interaction of beams.

4.5. Flexural-torsional buckling of concentrically loaded angle struts

This example, analyzed theoretically and numerically by Kitipornchai and Chan [22] and Kitipornchai and Lee [49], studies the elastic and inelastic flexural-torsional buckling load of concentrically loaded, pin-ended unequal-leg angle struts (L76x51x5 mm). The material properties are: Young's modulus of elasticity E = 200,000 MPa, Poisson's ratio $\nu = 0.3$, and yielding stress $F_{\nu} = 312$ MPa. Fig. 16 shows the elastic buckling factors for members with different modified slenderness. The definition of modified slenderness is $\lambda = \sqrt{F_v/(\pi^2 E)} L/r_{min}$, where L is the length of the angle bar and r_{min} is the minimum radius of gyration. In the figure, P_c is the applied axial load and P_v is the section yielding load (squash load). Twenty new displacement-based elements are used to simulate this flexural-torsional buckling behavior. It is shown that the buckling loads computed form the newly developed element coincide well with the theoretical values. Since the default reference line of the new element is the shear center axis, the rigid offsets developed in Section 3.7 are utilized to move the element reference line to centroidal axis so that the concentric loading condition

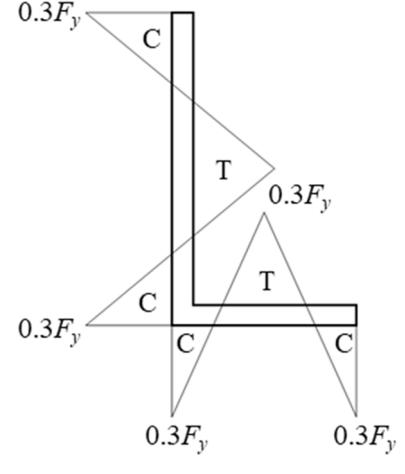
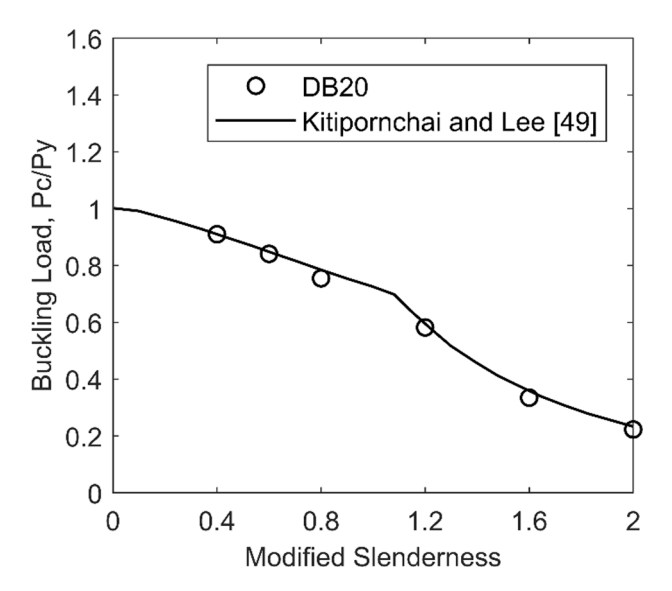


Fig. 17. Assumed residual stress distribution for angle sections.



 $\begin{tabular}{lll} Fig. & 18. Flexural-torsional & buckling & of & concentrically & loaded & angle struts (inelastic). \end{tabular}$

is satisfied.

For the inelastic buckling case, the idealized residual stress distribution shown in Fig. 17 is used both in the research of Kitipornchai and Lee [49] and in the present simulation. An elastic-perfectly plastic stress–strain curve is employed, while in the plastic region the shear modulus is assumed to remain unchanged. In the calculation of inelastic buckling loads, Kitipornchai and Lee [49] utilized a simplified mathematical model similar to that proposed by Trahair and Kitipornchai [50] for inelastic buckling of steel I-beams. Using the new displacement-based and mixed elements, the inelastic buckling loads of the angle struts with different slenderness are calculated and then compared with the results of Kitipornchai and Lee [49] in Fig. 18.

4.6. Cantilever with angle section subjected to an eccentric axial force

This example, studied numerically by several researchers [23,30,51], addresses a cantilever beam with asymmetric cross section subjected to an eccentric axial force P. The cantilever is fixed at the left end in Fig. 19. The axial force P is applied to the shear center of the free end. As shown in Fig. 19, the geometric and material properties of the cantilever are: L=1,400 mm, a=76 mm, b=51 mm, t=6.5 mm, Young's modulus t=1,100 mm, t=1,100 mm,

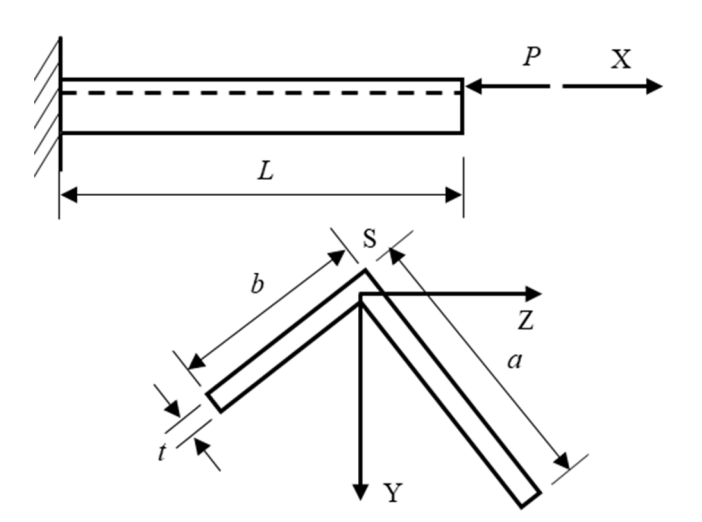


Fig. 19. Cantilever with asymmetric angle section subjected to an eccentric axial force.

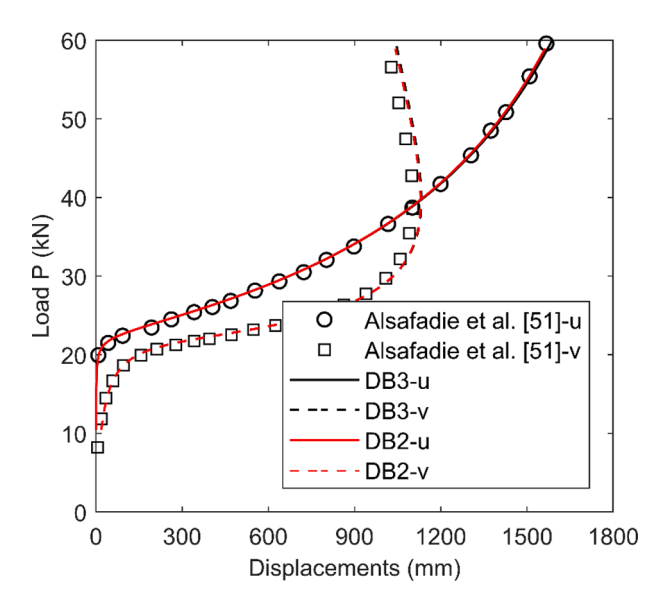


Fig. 20. Cantilever with asymmetric angle section: load-deflection u and v curves.

193.05 GPa and Poisson's ratio $\nu=0.3$. The load–deflection curves of the present study together with the results of Alsafadie et al. [51] are plotted in Fig. 20, in which the axial displacement u and lateral displacement v in Y direction are presented. As seen in this figure, three new displacement-based elements in the present study are enough to obtain relatively accurate results, while Alsafadie et al. [51] utilized 30 displacement-based elements to get similar results.

4.7. Lateral-torsional buckling of a cantilever with tee section

This example is part of the buckling studies on cantilever beams subjected to an end force conducted by several researchers [29,52–55]. Two cases, 4Ba65 and 4Ba50, in their research are simulated using the element developed in the present study. Here, 4Ba65 means that a tee section is used, a larger flange is at the top, the load acts at the upper face, and the length of the cantilever is L=65 in; while 4Ba50 means the same as 4Ba65 except for the length is L=50 in. The loading and geometry properties are shown in Fig. 21 with b=1.239 in., $t_f=0.1236$ in., h=2.8292 in., and $t_w=0.0863$ in. The buckling loads obtained using 5 elements developed in the present study are shown in Table 1

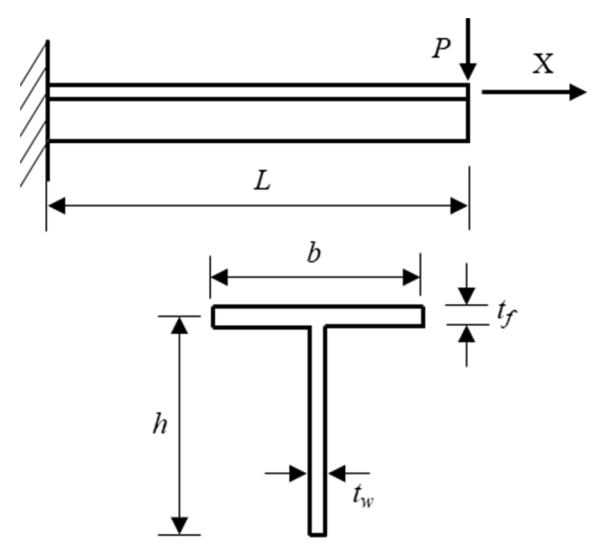


Fig. 21. Cantilever beam subjected to an end force.

Table 1Buckling loads of cantilever beams subjected to an end force.

Case	Buckling loads (lb)						
	Exp. [55]	Theory [55]	FEM [54]	FEM [52,53]	Present		
4Ba65 4Ba50	21.2 33.6	21.4 32.7	21.1 32.1	21.6 33.2	21.2 32.4		

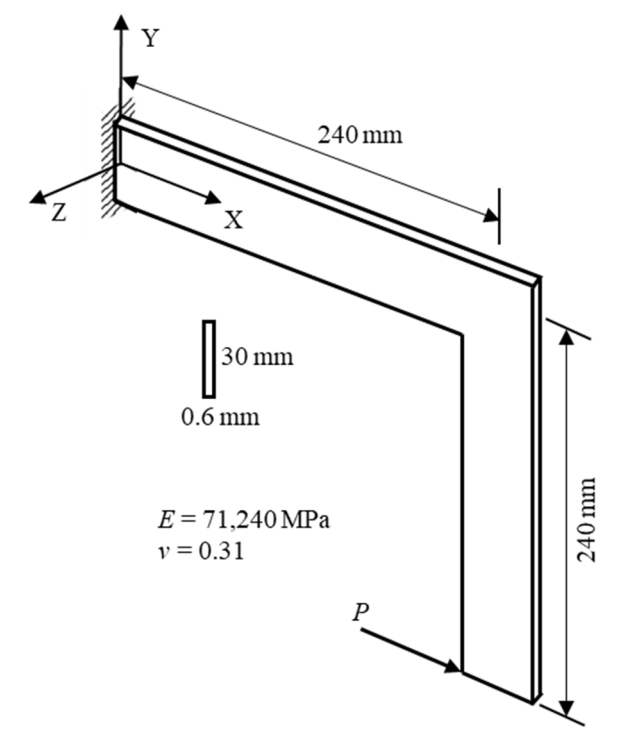


Fig. 22. Right-angled frame subjected to an end load.

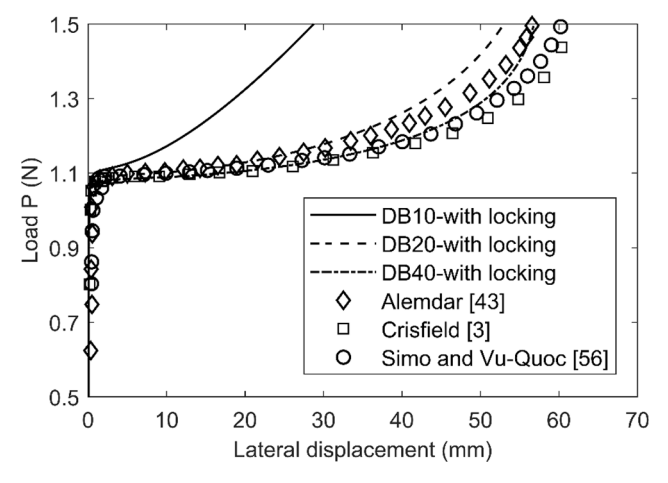


Fig. 23. Load/tip Z-displacement for right-angled frame (with membrane locking).

together with the results from other researchers for comparison, which proves the accuracy of the new element in the prediction of buckling loads.

4.8. Buckling of a right-angled frame subjected to an end load

The right-angled frame shown in Fig. 22 was analyzed by many

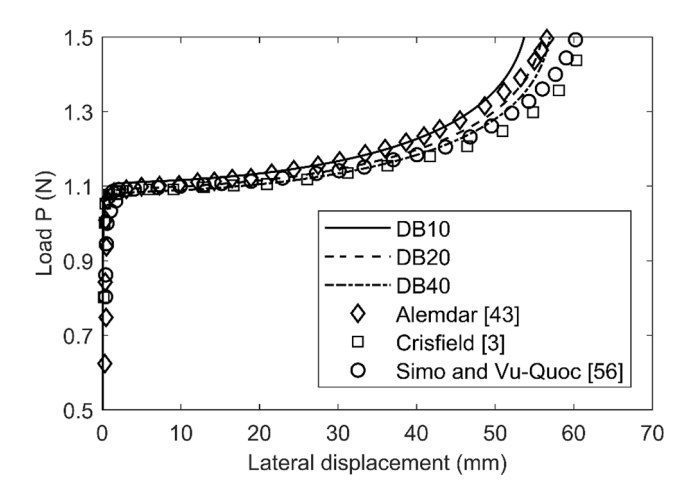


Fig. 24. Load/tip Z-displacement for right-angled frame (with membrane locking remedied).

authors [3,41,43,56]. The load P is applied in the X-direction at the member tip with a very small perturbation load of 0.0002 N in the Z-direction at the tip to induce buckling artificially. At first, the problem is solved using the new element with membrane locking, the computed response of the applied load P and the tip deflection in the Z-direction is plotted in Fig. 23 together with other results of this work. It is shown that due to membrane locking, more than 20 elements in total are needed for the two members to get comparable results with other work. If fewer elements are used, the post-buckling stiffness is overestimated dramatically.

However, if the new element with membrane locking remedied is used, only 10 elements in total are enough to obtain an accurate response (see Fig. 24). Thus, it may be accepted that the adopted methodology can remove membrane locking and improve the results significantly.

4.9. Flexural-torsional buckling of a tee beam

This example addresses flexural—torsional buckling of a tee beam under axial load considering both elastic and inelastic material. Battini and Pacoste [32] conducted numerical study of this example as shown in

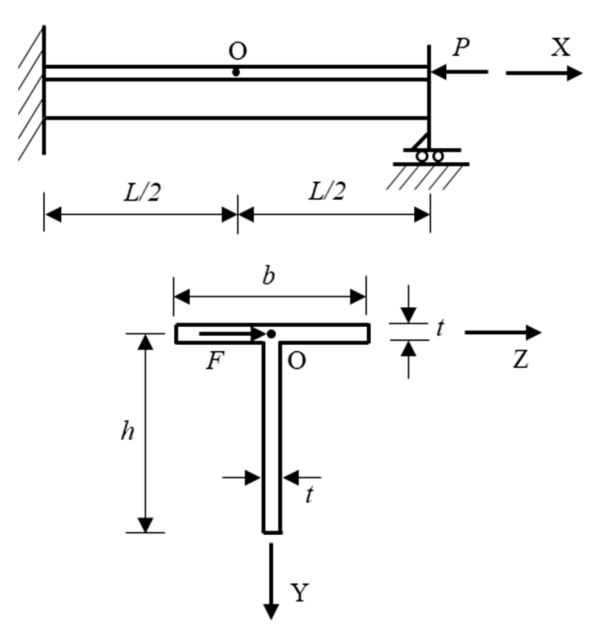


Fig. 25. Flexural-torsional buckling of a tee beam.

Fig. 25 with the following geometric material properties: $L=1,800,\,h=b=60,\,t=6,\,$ Young's modulus $E=70,000,\,$ Poisson's ratio $\nu=0.33,\,$ yielding stress $F_y=20,\,$ and post-yield strain hardening modulus $E_t=E/5.\,$ For the inelastic case, a bilinear plastic constitutive relation is assumed. The left end of the beam is fixed and only the axial displacement is allowed at the right end. A compressive axial force P is applied at the shear center of the right end. In addition, a small perturbation force F=P/1000 is introduced at the midspan point in the Z-direction. In the present research, 4 and 8 elements with 304 fibers in the cross section are used to simulate the buckling and yielding behavior. Note that Battini and Pacoste [32] used 40 displacement-based elements in their simulation.

The load/Z-displacement curves of point O in both elastic and inelastic cases are shown in Fig. 26 and Fig. 27, respectively. The agreement between the present simulation results and the results of Battini and Pacoste [32] is very good, but fewer elements are needed for the element in this work.

4.10. Lee's frame

Lee et al. [57] investigated a structural frame represented in Fig. 28, using a linear elastic material and neglecting axial deformations. Several other researchers numerically studied this structure also assuming linear elastic material [56,58,59]. de Souza [41] and Cichoń [60] analyzed this example for both elastic and inelastic materials. In the present study, the bilinear elasto-plastic material model with kinematic hardening presented in de Souza [41] is adopted for the inelastic case (see Fig. 28 for the material properties). Weak axis bending is used for both the horizontal and vertical members.

The frame is first analyzed using the new displacement-based element with membrane locking for both elastic and inelastic cases. Fig. 29 and Fig. 30 compare the load displacement curves for the elastic case and inelastic case, respectively. It can be seen that 20 elements (10 elements per member) with membrane locking still produce over stiff results, while 40 elements can give results with sufficient accuracy. If only 10 elements with membrane locking are used, the results will be severely inaccurate (too stiff), so they are not shown in the figures. This example shows that for the displacement-based element considering high order strain terms, the membrane locking problem must be addressed, otherwise more elements are needed to obtain accurate results.

The frame is then analyzed using the displacement-based element with membrane locking remedied. Fig. 31 and Fig. 32 illustrate the results from the present study and those from de Souza [41]. It can be

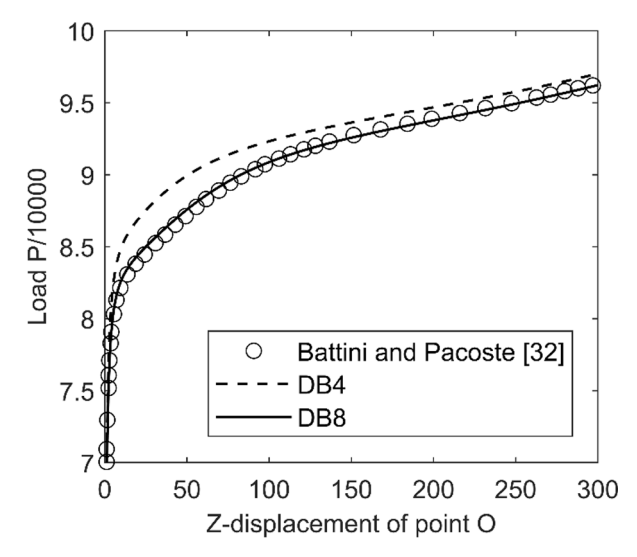


Fig. 26. Load/Z-displacement of point O curve (elastic case).

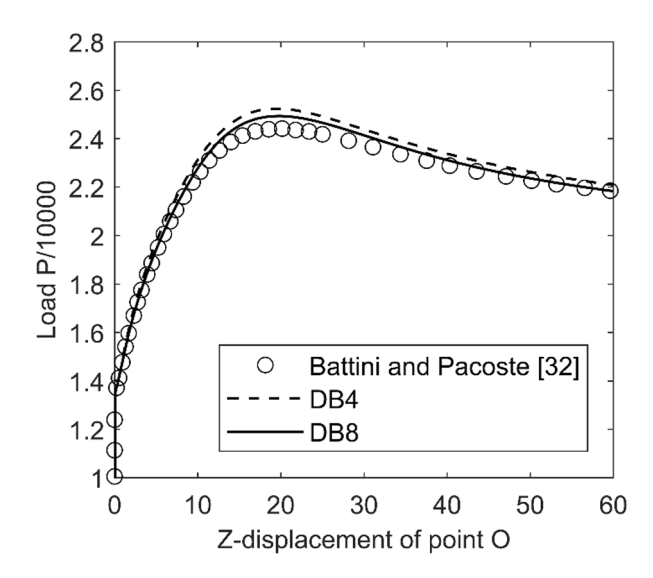


Fig. 27. Load/Z-displacement of point O curve (inelastic case).

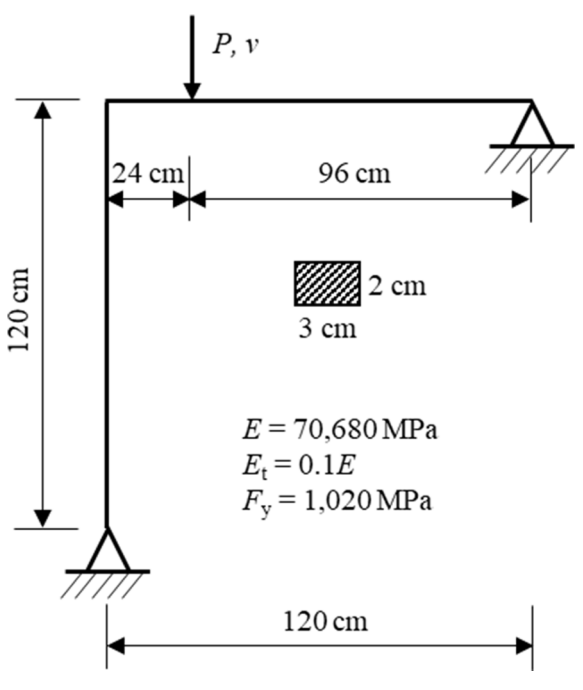


Fig. 28. Lee's frame.

concluded that the displacement-based element with membrane locking remedied can reduce the required elements amount to only 5, compared with the displacement-based element with membrane locking. For "DB5" in Fig. 31 and Fig. 32, three elements are used for the horizontal member and two elements are used for the vertical member. For "DB4", three elements are used for the horizontal member and one element is used for the vertical member.

4.11. Buckling of unequal-leg angles with fixed ends

This example studies the buckling behavior of four unequal-leg angles. An experimental investigation of the angles was conducted by Dinis et al. [61]. Dinis et al. [61] and Liu et al. [28] also analyzed this example numerically using shell elements and beam elements, respectively. According to Dinis et al. [61], the steel angles were made of dual grade A36-Grade50 steel with the following material properties: Young's modulus E=207 GPa, Poisson's ratio $\nu=0.3$, and yielding stress $F_{\gamma}=1$

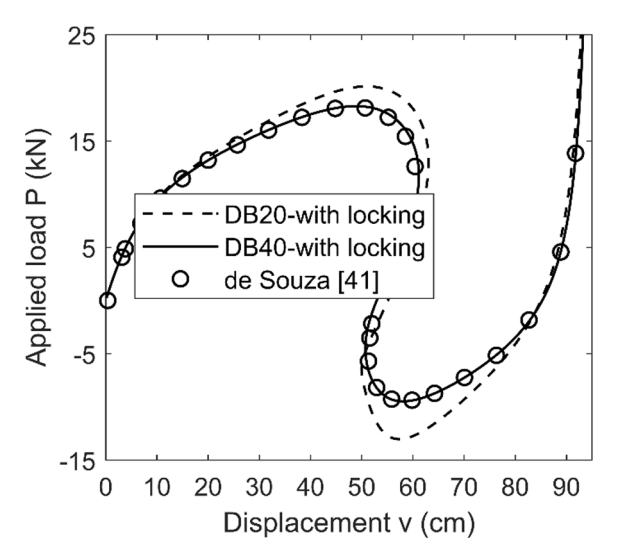


Fig. 29. Equilibrium path for Lee's frame (element with membrane locking, elastic).

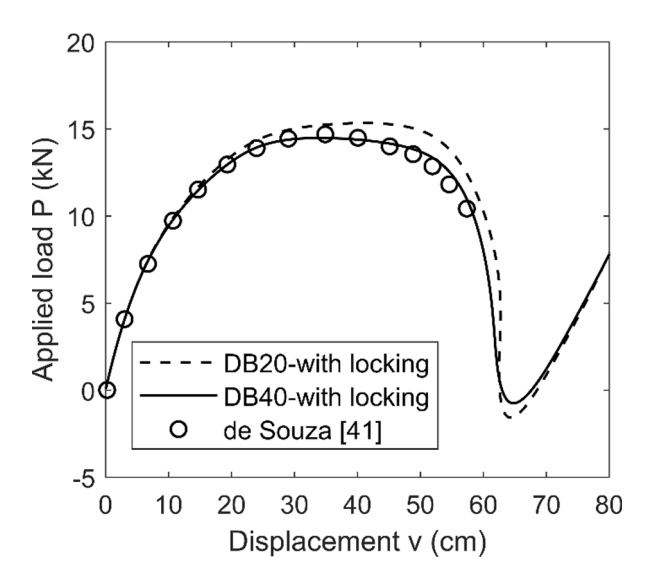


Fig. 30. Equilibrium path for Lee's frame (element with membrane locking, inelastic).

379 MPa. The measurements of the cross section dimensions and member lengths are listed in Table 2, where B_L and B_S are lengths of the long leg and short leg, respectively; t_L and t_S are thicknesses of the long led and short leg, respectively; and L is the member length. The member ends are fixed and only the axial translation of the loaded end is possible. Note that the angle members are loaded concentrically, which means the axial load is applied to the centroid of the cross section.

The comparison of load–displacement curves of the four specimens obtained from experimental and numerical studies is shown in Figs. 33 to 36. It is seen that the buckling loads can be estimated accurately using the displacement-based element in this work. In addition, this element can give a better estimation of the post-buckling behavior for the longer specimens (L72 and L60) than the shorter specimens. This may be because the shear deformation is significant for shorter specimens and section distortion may happen at large deformation, which are not considered in this element.

5. Conclusions

A geometrically and materially nonlinear displacement-based

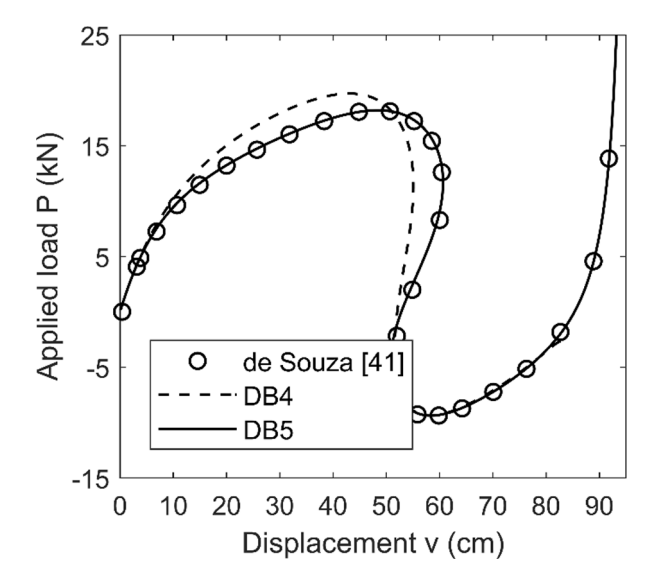


Fig. 31. Equilibrium path for Lee's frame (element with membrane locking remedied, elastic).

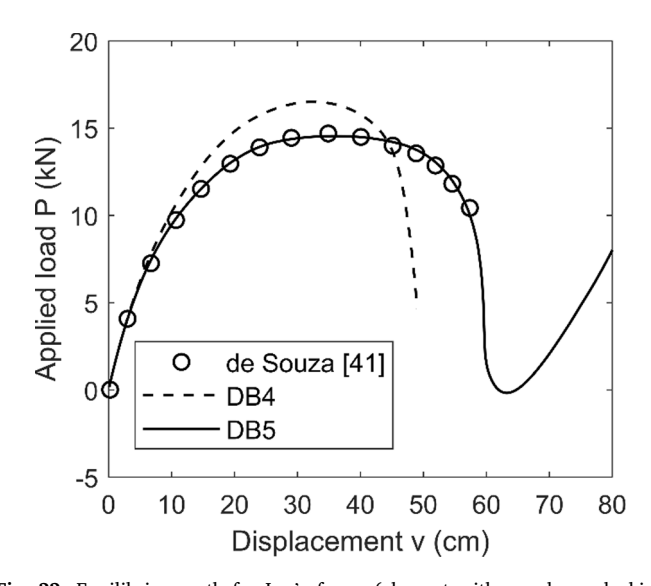


Fig. 32. Equilibrium path for Lee's frame (element with membrane locking remedied, inelastic).

Table 2
Specimen geometries of unequal-leg angles.

Specimen	B_L (mm)	t_L (mm)	B_S (mm)	t_S (mm)	L (mm)
L48A	126.6	6.5	76.9	6.5	1224.0
L48B	126.6	6.6	76.7	6.5	1219.2
L60	126.5	6.6	76.7	6.6	1525.6
L72	126.5	6.6	76.8	6.5	1828.8

element for structural members with angle and tee sections has been developed and validated in this work. The geometric nonlinear phenomenon is simulated by using the corotational transformation, and by adopting the total Lagrangian formulation in the basic system through employing Green-Lagrange strains. Consequently, the newly developed element is able to take into account the axial-flexural-torsional interaction behavior of structural members in large deformation. In order to model members with asymmetric sections, the element DOFs are defined with respect to both centroid and shear center in the basic system, and then transformed to the shear center in advance of the corotational

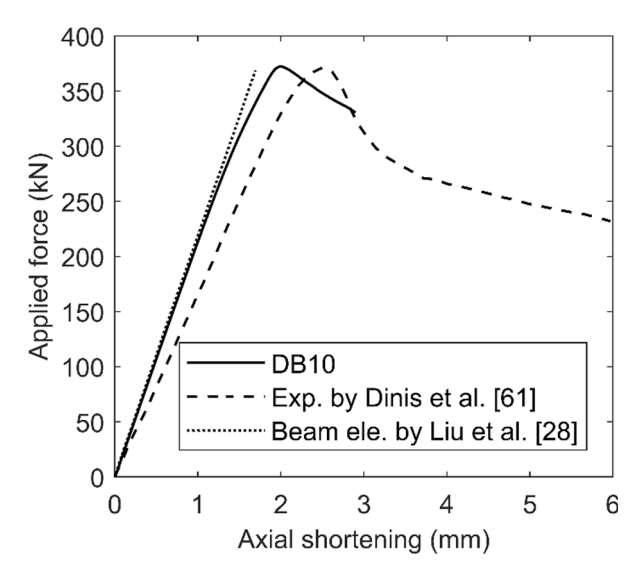


Fig. 33. Load-displacement curves of unequal-leg angles (L48A).

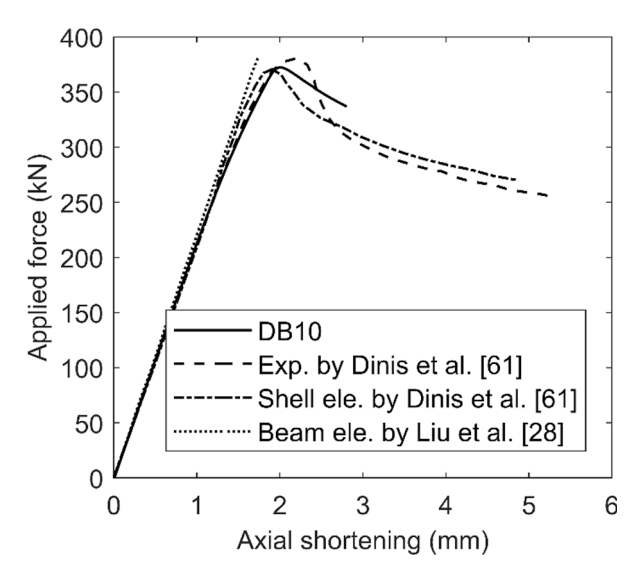


Fig. 34. Load-displacement curves of unequal-leg angles (L48B).

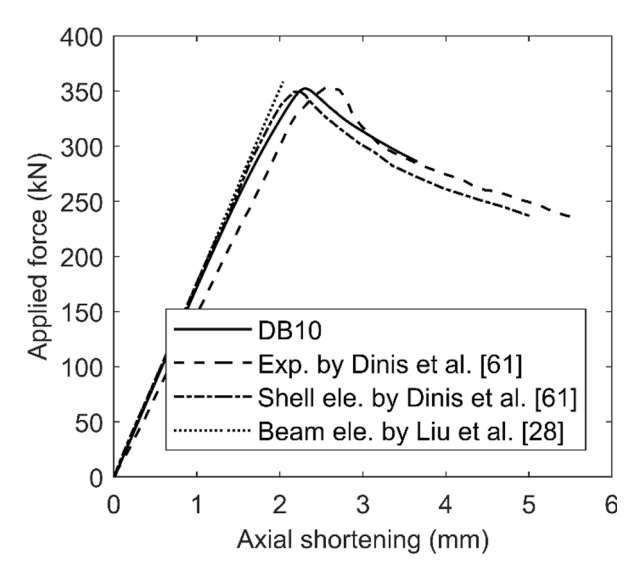


Fig. 35. Load-displacement curves of unequal-leg angles (L60).

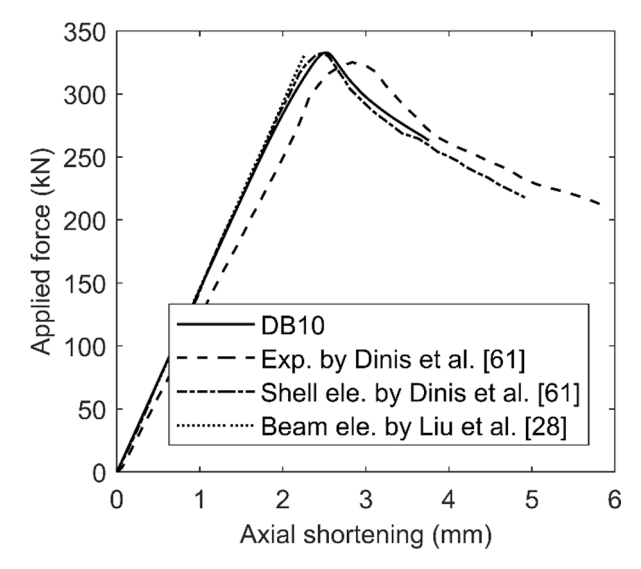


Fig. 36. Load-displacement curves of unequal-leg angles (L72).

transformation. The material nonlinearity is considered by discretizing the member cross section into fibers and applying the uniaxial constitutive law and numerical integration to calculate cross-section forces. Examples show that nonlinear torsion, elastic and inelastic flexural—torsional buckling, and lateral-torsional buckling can be modeled accurately with only a small number of elements. The displacement-based element yields overestimated stiffness for both elastic and inelastic inextensional bending modes unless the membrane locking phenomenon is remedied. With the approach adopted in this work to alleviate membrane locking, the improved version of the displacement-based element presents excellent performance for a comprehensive set of structural members and frames.

CRediT authorship contribution statement

Xinlong Du: Methodology, Software, Validation, Writing - original draft. **Jerome Hajjar:** Conceptualization, Writing - review & editing.

Declaration of Competing Interest

The authors declare that they have no known competing financial interests or personal relationships that could have appeared to influence the work reported in this paper.

Acknowledgement

This research is supported by the National Science Foundation under Grant No. CRISP-1638234 and Northeastern University. This support is gratefully acknowledged.

Appendix A. Linearization of the governing equation

This appendix shows details of the linearization process of the governing equation to derive the tangent stiffness matrix and internal forces, which are used in Section 3.4. Using a Taylor series expansion to Eq. (42) and neglecting the high order terms, the following equation is obtained

$$\mathbf{g}^{i+1} pprox \mathbf{g}^{i} + \frac{d}{d\alpha}|_{\alpha,\beta=0}\mathbf{g}\left(\mathbf{D}_{b}^{i} + \alpha\Delta\mathbf{D}_{b}\right) + \frac{d}{d\beta}|_{\alpha,\beta=0}\mathbf{g}\left(\mathbf{P}_{ext}^{i} + \beta\Delta\mathbf{P}_{ext}\right) = 0$$
 (A.1)

where α and β are scalers used to scale vectors ΔD_b and ΔP_{ext} . Variables

with a superscript i or (i + 1) represent their values in the ith or (i + 1)th iteration. The terms in the above equation are obtained as shown below

$$\frac{d}{d\alpha}|_{\alpha,\beta=0}\mathbf{g}\left(\mathbf{D}_{b}^{i} + \alpha\Delta\mathbf{D}_{b}\right) = \int_{l_{0}} \frac{d}{d\alpha}|_{\alpha,\beta=0}\left(N_{\delta d2}^{T}\right)N_{\delta d1}^{T}\mathbf{S}dx + \int_{l_{0}} N_{\delta d2}^{T}\frac{d}{d\alpha}|_{\alpha,\beta=0}\left(N_{\delta d1}^{T}\right)\mathbf{S}dx + \int_{l_{0}} N_{\delta d2}^{T}N_{\delta d1}^{T}\frac{d}{d\alpha}|_{\alpha,\beta=0}(\mathbf{S})dx$$

$$= \int_{l_{0}} N_{\delta d2}^{T}\mathbf{G}N_{\delta d2}dx\Delta\mathbf{D}_{b} + \int_{l_{0}} N_{\delta d2}^{T}N_{\delta d1}^{T}\mathbf{K}_{s}N_{\delta d1}N_{\delta d2}dx\Delta\mathbf{D}_{b} \tag{A.2}$$

where the following relations are used

$$\frac{d}{da}|_{\alpha,\beta=0}(N_{\delta d2}^T)=0\tag{A.3}$$

$$\frac{d}{d\alpha}|_{\alpha,\beta=0} (N_{\delta d1}^T) S = \frac{dN_{\delta d1}^T}{d(\alpha \Delta \mathbf{D}_b)} \frac{d(\alpha \Delta \mathbf{D}_b)}{d\alpha} S = G \frac{d\mathbf{v}}{d(\alpha \Delta \mathbf{D}_b)} \Delta \mathbf{D}_b = G N_{\delta d2} \Delta \mathbf{D}_b$$
(A.4)

$$\frac{d}{d\alpha}|_{\alpha,\beta=0}(S) = \frac{dS}{d(\alpha\Delta\mathbf{D}_b)} \frac{d(\alpha\Delta\mathbf{D}_b)}{d\alpha} = \int_{A_0} \mathbf{Y}^T \frac{d\mathbf{\sigma}}{d(\alpha\Delta\mathbf{D}_b)} dA\Delta\mathbf{D}_b = \int_{A_0} \mathbf{Y}^T \mathbf{E} \frac{d\epsilon}{d(\alpha\Delta\mathbf{D}_b)} dA\Delta\mathbf{D}_b = \int_{A_0} \mathbf{Y}^T \mathbf{E} \mathbf{Y} \mathbf{N}_{\delta d1} \mathbf{N}_{\delta d2} dA\Delta\mathbf{D}_b = \int_{A_0} \mathbf{Y}^T \mathbf{E} \mathbf{Y} dA\mathbf{N}_{\delta d1} \mathbf{N}_{\delta d2} \Delta\mathbf{D}_b$$

$$= \mathbf{K}_{\bullet} \mathbf{N}_{\delta d1} \mathbf{N}_{\delta d2} \Delta\mathbf{D}_b \tag{A.5}$$

in which

$$G = \begin{bmatrix} 0 & 0 & 0 & 0 & 0 & 0 & 0 \\ 0 & N & 0 & 0 & 0 & 0 & Nz_s \\ 0 & 0 & N & 0 & 0 & 0 & -Ny_s \\ 0 & 0 & 0 & 0 & 0 & M_y & 0 \\ 0 & 0 & 0 & 0 & M_z & 0 \\ 0 & 0 & 0 & M_y & M_z & 0 & 0 \\ 0 & Nz_s & -Ny_s & 0 & 0 & 0 & W \end{bmatrix}$$
(A.6)

$$\mathbf{K}_{s} = \int_{A_{0}} \mathbf{Y}^{T} \mathbf{E} \mathbf{Y} dA = \int_{A_{0}} \begin{bmatrix} E & -yE & zE & p^{2}E & 0 \\ -yE & y^{2}E & -yzE & -p^{2}yE & 0 \\ zE & -yzE & z^{2}E & p^{2}zE & 0 \\ p^{2}E & -p^{2}yE & p^{2}E & p^{4}E & 0 \\ 0 & 0 & 0 & 4n^{2}G \end{bmatrix} dA$$
(A.7)

in which

$$p^{2} = (y - y_{s})^{2} + (z - z_{s})^{2}$$
(A.8)

Here, K_s is the section stiffness matrix. The matrix E sets the constitutive relation between the stresses and strains. Here

$$E = \begin{bmatrix} E & 0 \\ 0 & G \end{bmatrix} \tag{A.9}$$

where E is the tangent Young's modulus and G is the shear modulus.

In addition,

$$\frac{d}{d\beta}|_{\alpha,\beta=0}\mathbf{g}(\mathbf{Q}_{ext}^{i}+\beta\Delta\mathbf{P}_{ext}) = \frac{d\mathbf{g}}{d(\beta\Delta\mathbf{P}_{ext})}\frac{d(\beta\Delta\mathbf{P}_{ext})}{d\beta} = -\Delta\mathbf{P}_{ext}$$
(A.10)

Therefore, the following relation is obtained

$$\mathbf{g}^{i} + \int_{l_0} \mathbf{N}_{\delta d2}^{T} \mathbf{G} \mathbf{N}_{\delta d2} dx \Delta \mathbf{D}_{b} + \int_{l_0} \mathbf{N}_{\delta d2}^{T} \mathbf{X}_{s} \mathbf{N}_{\delta d1} \mathbf{X}_{s} \mathbf{N}_{\delta d1} \mathbf{N}_{\delta d2} dx \Delta \mathbf{D}_{b} - \Delta \mathbf{P}_{ext} = 0$$
(A.11)

which can be expressed as the following equation with the help of Eq. (42)

$$\left(\int_{l_0} N_{\delta d2}^T G N_{\delta d2} dx + \int_{l_0} N_{\delta d2}^T N_{\delta d1}^T K_s N_{\delta d1} N_{\delta d2} dx\right) \Delta \boldsymbol{D}_b = \Delta \boldsymbol{P}_{ext} + \boldsymbol{P}_{ext}^i - \int_{l_0} N_{\delta d2}^T N_{\delta d1}^T S^i dx \tag{A.12}$$

This iteration equation can be expressed in short as shown in Eq. (43).

Appendix B. The transformation for rigid offsets

This appendix shows details of the transformation used to consider eccentricities as discussed in Section 3.7. From the equilibriums on rigid offsets 1-*I* and 2-*J* (see Fig. 6), the following transformation for the end forces of the element reference ends P and the end forces at the shear centers \hat{P} is obtained

$$\boldsymbol{P} = \boldsymbol{T}_{\text{off}}^{T} \widehat{\boldsymbol{P}}$$
 (B.1)

where the transformation matrix is given by

According to the principle of virtual work, the contragredient transformation of the end displacements is obtained as this tangential relationship

$$\delta \widehat{D} = T_{off} \delta D$$
 (B.3)

where D denotes the end displacements of the element reference ends. Small rotations are assumed in the derivations in this section. With $\delta \hat{P} = \hat{K} \delta \hat{D}$, as developed in Section 2.2, we have

$$\delta P = T_{off}^T \delta \hat{P} = T_{off}^T \hat{K} \delta \hat{D} = T_{off}^T \hat{K} T_{off} \delta D = K \delta D$$
(B.4)

where $K = T_{off}^T \hat{K} T_{off}$ is the tangent stiffness matrix in the global system considering rigid offsets.

References

- [1] Bathe KJ. Finite element procedures. Klaus-Jurgen Bathe 2006.
- [2] Bathe KJ, Bolourchi S. Large displacement analysis of three-dimensional beam structures. Int J Numer Meth Eng 1979;14:961–86.
- [3] Crisfield MA. A consistent co-rotational formulation for non-linear, threedimensional, beam-elements. Comput Methods Appl Mech Eng 1990;81:131–50.
- [4] Crisfield MA. Non-linear finite element analysis of solids and structures. Chichester: John Wiley & Sons; 1991.
- [5] Crisfield MA. Non-linear finite element analysis of solids and structures Advanced Topics. Chichester: John Wiley & Sons; 1997.
- [6] Yang Y-B, Kuo S-R. Theory and analysis of nonlinear framed structures. Singapore: Prentice Hall; 1994.
- [7] Mattiasson K, Bengtsson A, Samuelsson A. On the accuracy and efficiency of numerical algorithms for geometrically nonlinear structural analysis. In: Bergan PG, Bathe KJ, Wunderlich W, editors. Europe-US Symposium on Finite Element Methods for Nonlinear Problems. Trondheim, Norway: Springer-Verlag; 1985.
- [8] Baigent AH, Hancock GJ. Structural analysis of assemblages of thin-walled members. Eng Struct 1982;4:207–16.
- [9] Gruttmann F, Sauer R, Wagner W. Theory and numerics of three-dimensional beams with elastoplastic material behaviour. Int J Numer Meth Eng 2000;48: 1675–702.
- [10] Pi YL, Trahair NS. Nonlinear inelastic analysis of steel beam-columns. I: Theory. J Struct Eng 1994;120:2041–61.
- [11] Simo JC, Vu-Quoc L. A geometrically-exact rod model incorporating shear and torsion-warping deformation. Int J Solids Struct 1991;27:371–93.
- [12] Vlasov VZ. Thin-walled elastic beams. Jerusalem: Israel Program for Scientific Translations 1961.
- [13] Yang Y-B, McGuire W. Stiffness matrix for geometric nonlinear analysis. J Struct Eng 1986:112:853–77.
- [14] Dinis PB, Camotim D, Silvestre N. GBT formulation to analyse the buckling behaviour of thin-walled members with arbitrarily 'branched' open cross-sections. Thin-Walled Structures. 2006;44:20–38.
- [15] Gonçalves R, Ritto-Corrêa M, Camotim D. A new approach to the calculation of cross-section deformation modes in the framework of generalized beam theory. Comput Mech 2010;46:759–81.
- [16] Martins AD, Camotim D, Dinis PB. Distortional-global interaction in lipped channel and zed-section beams: Strength, relevance and DSM design. Thin-Walled Structures. 2018;129:289–308.
- [17] Martins AD, Camotim D, Gonçalves R, Dinis PB. On the mechanics of localdistortional interaction in thin-walled lipped channel beams. Thin-Walled Structures. 2018;128:108–25.
- [18] Schardt R. Generalized beam theory—an adequate method for coupled stability problems. Thin-walled structures. 1994;19:161–80.
- [19] Zhang X, Rasmussen KJ, Zhang H. Beam-element-based analysis of locally and/or distortionally buckled members: Application. Thin-Walled Structures. 2015;95: 127–37.
- [20] Rasmussen KJ, Zhang X, Zhang H. Beam-element-based analysis of locally and/or distortionally buckled members: Theory. Thin-Walled Struct 2016;98:285–92.

- [21] Rasmussen K. Bifurcation of locally buckled members. Thin-Walled Struct 1997;28: 117–54.
- [22] Kitipornchai S, Chan S. Nonlinear finite element analysis of angle and tee beamcolumns. J Struct Eng 1987;113:721–39.
- [23] Chan S, Kitipornchai S. Geometric nonlinear analysis of asymmetric thin-walled beam-columns. Eng Struct 1987;9:243–54.
- [24] Al-Bermani FG, Kitipornchai S. Elasto-plastic large deformation analysis of thinwalled structures. Eng Struct 1990;12:28–36.
- [25] Lee P-S, McClure G. A general three-dimensional L-section beam finite element for elastoplastic large deformation analysis. Comput Struct 2006;84:215–29.
- [26] Liu S-W, Ziemian RD, Chen L, Chan S-L. Bifurcation and large-deflection analyses of thin-walled beam-columns with non-symmetric open-sections. Thin-Walled Struct 2018:132:287–301.
- [27] Ziemian RD, McGuire W, Liu SW. MASTAN2 v4.0. 2019.
- [28] Liu S-W, Gao W-L, Ziemian RD. Improved line-element formulations for the stability analysis of arbitrarily-shaped open-section beam-columns. Thin-Walled Struct 2019;144:106290.
- [29] Hsiao KM, Lin WY. A co-rotational formulation for thin-walled beams with monosymmetric open section. Comput Meth Appl Mech Eng 2000;190:1163–85.
- [30] Chen HH, Lin WY, Hsiao KM. Co-rotational finite element formulation for thinwalled beams with generic open section. Comput Methods Appl Mech Eng 2006; 195:2334–70.
- [31] Battini J-M, Pacoste C. Co-rotational beam elements with warping effects in instability problems. Comput Meth Appl Mech Eng 2002;191:1755–89.
- [32] Battini J-M, Pacoste C. Plastic instability of beam structures using co-rotational elements. Comput Methods Appl Mech Eng 2002;191:5811–31.
- [33] Rinchen, Hancock GJ, Rasmussen KJ. Formulation and implementation of general thin-walled open-section beam-column elements in OpenSees. Research Report R961: The University of Sydney, Australia; 2016.
- [34] Rinchen, Hancock GJ, Rasmussen KJ. Geometric and material nonlinear analysis of thin-walled members with arbitrary open cross-section. Thin-Walled Struct 2020; 153:106783.
- [35] McKenna F, Scott MH, Fenves GL. Nonlinear finite-element analysis software architecture using object composition. J Comput Civil Eng 2010;24:95–107.
- [36] Belytschko T, Liu WK, Moran B, Elkhodary K. Nonlinear finite elements for continua and structures. John wiley & sons; 2013.
- [37] Garcea G, Madeo A, Casciaro R. The implicit corotational method and its use in the derivation of nonlinear structural models for beams and plates. J Mech Mater Struct 2012;7:509–38.
- [38] Garcea G, Madeo A, Casciaro R. Nonlinear FEM analysis for beams and plate assemblages based on the implicit corotational method. J Mech Mater Struct 2012; 7:539–74.
- [39] Genoese A, Genoese A, Bilotta A, Garcea G. A geometrically exact beam model with non-uniform warping coherently derived from the Saint Venant rod. Eng Struct 2014;68:33–46.
- [40] Mattiasson K. On the co-rotational finite element formulation for large deformation problems: Department of Structural Mechanics. Chalmers University of Technology; 1983.
- [41] de Souza RM. Force-based finite element for large displacement inelastic analysis of frames [PhD Thesis]. USA: University of California, Berkeley; 2000.

- [42] Hancock G. Portal frames composed of cold-formed channel-and Z-sections. Steel Framed Structures - Stability and Strength. England: Taylor & Francis; 2005. p. 230–64.
- [43] Alemdar BN. Distributed plasticity analysis of steel building structural systems. USA: Georgia Institute of Technology; 2001 [PhD Thesis].
- [44] Trahair NS. Flexural-torsional buckling of structures. first ed. Boca Raton: CRC Press; 1993.
- [45] Trahair NS. Nonlinear elastic nonuniform torsion. J Struct Eng 2005;131:1135-42.
- [46] McGuire W, Gallagher RH, Ziemian RD. Matrix Structural Analysis. John Wiley & Sons; 2000.
- [47] Gregory M. A nonlinear bending effect when certain unsymmetrical sections are subjected to a pure torque: Department of Civil Engineering. University of Tasmania; 1960.
- [48] Engel H, Goodier J. Measurements of torsional stiffness changes and instability due to tension, compression, and bending. J Appl Mech-Trans ASME. 1953;20:553–60.
- [49] Kitipornchai S, Lee H. Inelastic buckling of single-angle, tee and double-angle struts. J Constr Steel Res 1986;6:3–20.
- [50] Trahair NS, Kitipornchai S. Buckling of inelastic I-beams under uniform moment. J Struct Div 1972;98.
- [51] Alsafadie R, Hjiaj M, Battini J-M. Corotational mixed finite element formulation for thin-walled beams with generic cross-section. Comput Methods Appl Mech Eng 2010:199:3197–212.

- [52] Pi YL, Trahair NS. Prebuckling deflections and lateral buckling. II: applications. J Struct Eng 1992;118:2967–85.
- [53] Pi YL, Trahair NS. Prebuckling deflections and lateral buckling. I: theory. J Struct Eng 1992;118:2949–66.
- [54] Attard MM. Lateral buckling analysis of beams by the FEM. Comput Struct 1986; 23:217–31.
- [55] Anderson JM, Trahair NS. Stability of monosymmetric beams and cantilevers. J Struct Div 1972.
- [56] Simo JC, Vu-Quoc L. A three-dimensional finite-strain rod model. Part II: Computational aspects. Comput Meth Appl Mech Eng 1986;58:79–116.
- [57] Lee S-L, Manuel FS, Rossow EC. Large deflections and stability of elastic frame. J Eng Mech Div 1968;94:521–48.
- [58] Pacoste C, Eriksson A. Beam elements in instability problems. Comput Methods Appl Mech Eng 1997;144:163–97.
- [59] Chen H, Blandford GE. Work-increment-control method for non-linear analysis. Int J Numer Meth Eng 1993;36:909–30.
- [60] Cichoń C. Large displacements in-plane analysis of elastic-plastic frames. Comput Struct 1984;19:737-45.
- [61] Dinis PB, Camotim D, Belivanis K, Roskos C, Helwig T. On the Buckling, Post-Buckling and Strength Behavior of Thin-Walled Unequal-Leg Angle Columns. Proceedings of the Annual Stability Conference Structural Stability Research Council: Structural Stability Research Council Nashville, Tennessee. 2015.